



UNIONE EUROPEA
Fondo Sociale Europeo
Fondo Europeo di Sviluppo Regionale



Document ID

PON-OR1-01-TSP

Revision

01

Document classification

Preliminary technical specifications¹

Tender

Supply of a W-band multibeam heterodyne receiver for the Sardinia Radio Telescope.

Type of tender

Competitive Dialogue pursuant to art. 64 D.lgs. 18 april 2016, n. 50, and s.m.i.

Decision Act

Determinazione n. 183 - 9 agosto 2019

Tender value

€ 2.300.000,00

Funding source

PON "Ricerca e Innovazione 2014-2020" - Avviso D.D. 424 del 28/02/2018

PON FSE FESR / PIR01_00010 "SRT_HighFreq - Potenziamento del Sardinia Radio Telescope per lo studio dell'Universo alle alte frequenze"

CUP

C87E19000000007

CIG

8018611F1D

¹ This document is Intellectual Property of INAF and is extracted from an INAF Internal Report under publication. All rights reserved.

Acronyms:

1IF = First frequency down-conversion
 2IF = Second frequency down-conversion
 2SB = Sideband Separation
 AIV = Acceptance Integration Verification
 AR = Rack cabinet
 ASI = Italian Space Agency
 A/D = Analog to Digital
 BPF = Band pass filter
 BW = Bandwidth
 BWG = Beam wave guide
 CED = “Centro Elaborazione Dati” (Data Processing Center)
 CS = Conversion stage
 DBBC = Digital Baseband Converter
 DBE = Digital Back-end
 DFB = Digital Filter Bank
 DS = Distribution stage
 EER = Elevation Equipment Room
 F1 = Primary focus
 F2 = Secondary focus
 F3 = Beam waveguide focus
 FBCB = Full Band Conversion/Continuum Board/Back-end
 FoV = Field of View
 FPGA = Field-programmable gate array
 GPU = Graphics processing unit
 GRP = Gregorian Receiver Positioner
 GRR = Gregorian Receiver Room
 H/V = Horizontal/Vertical polarization
 HPF = High pass filter
 IF = Intermediate Frequency
 INAF = National Institute for Astrophysics, Italy
 LSB = Lower side band
 LNA = Low noise amplifier
 LO = Local oscillator
 M1 = Main reflector
 M2 = Secondary reflector
 M3 = Mirror for selection of BWG focus
 MS = Master synthesizer
 MMIC = Monolithic Microwave Integrated Circuit
 NDA = Non-Disclosure Agreement
 PAD = Fixed attenuator
 RF = Radio Frequency (meaning also sky band)
 RFI = Radio Frequency Interference
 RFoF = Radio Frequency over Fiber (intended to transport the 1IF band)
 SRT = Sardinia Radio Telescope
 SSB = Single Side Band
 Tripler = x 3 frequency multiplier
 TP = Total power
 USB = Upper side band
 VLBI = Very Long Baseline Interferometry
 WIDEBAND = low resolution but wideband spectrometer



UNIONE EUROPEA
Fondo Sociale Europeo
Fondo Europeo di Sviluppo Regionale



Index

1	EXECUTIVE SUMMARY	5
2	INTRODUCTION TO SRT	8
3	W-BAND RECEIVER ARCHITECTURE: NOISE AND IMAGE BAND REJECTION	11
4	MOUNTING OF THE ARRAY RECEIVER AT THE SRT GREGORIAN FOCUS	14
4.1	GREGORIAN FOCUS RECEIVER POSITIONER	14
4.2	MECHANICAL DEROTATOR AND CABLE WRAP	17
5	OPTICAL CONFIGURATION AND CRYOGENIC MODULES	19
5.1	SIZE OF FOCAL PLANE AT THE GREGORIAN FOCUS	20
5.2	FEED-SYSTEM (SINGLE CHAIN)	20
5.3	BASELINE W-BAND 3×3 RECEIVER ARRAY CONFIGURATION	22
5.4	W-BAND RECEIVER ARRAYS IN 4×4 AND 3×4 CONFIGURATIONS AND DESIGN OF MINIATURIZED CRYOGENIC MODULES	25
5.4.1	<i>Cryogenic array based on dual-polarization LNAs</i>	<i>28</i>
5.4.2	<i>Cryogenic array based on “active OMT”</i>	<i>29</i>
5.5	CRYOGENIC LOW NOISE AMPLIFIERS	29
6	RECEIVER ARCHITECTURE, DOWN-CONVERSION SCHEMES, POWER AND NOISE BUDGETS	30
6.1	3×3 ARRAY WITH SIDEBAND SEPARATING DOWN-CONVERTERS	31
6.2	4×4 ARRAY WITH SINGLE SIDE BAND DOWN-CONVERTERS	33
6.3	11F SIGNAL TRANSPORTATION AND INTEGRATION WITH OTHER RECEIVERS	35
6.4	RECEIVER POWER BUDGET	36
6.4.1	<i>Power budget with receiver looking at a room temperature load</i>	<i>36</i>
6.4.2	<i>Power budget with receiver looking at the cold sky</i>	<i>37</i>
6.4.3	<i>Power budget with receiver looking at the Sun through solar filters</i>	<i>37</i>
6.5	RECEIVER NOISE BUDGET	37
6.6	RECEIVER CALIBRATION	38
7	OVERALL MECHANICALS, ELECTRICAL AND ADDITIONAL REQUIREMENTS	39
7.1	MECHANICAL ARRANGEMENT	39
7.2	CRYOSTAT WITH CTI CRYOGENERATOR AND VACUUM COMPONENTS	41
7.2.1	<i>CRYOGENERATOR AND HELIUM GAS LINES</i>	<i>41</i>
7.2.2	<i>Vacuum window and Infrared filter</i>	<i>42</i>
7.2.3	<i>Cryostat and vacuum system</i>	<i>42</i>
7.2.4	<i>Monitor and control module</i>	<i>45</i>
7.3	LNA BIAS AND MONITOR&CONTROL	46
7.3.1	<i>Analogue LNA bias board</i>	<i>47</i>
7.3.2	<i>New digital LNA bias board</i>	<i>47</i>
7.4	DOWN-CONVERTER MODULE(S)	49
7.5	MECHANICAL DEROTATOR AND DEWAR INTERFACE	50
7.6	SOLAR FILTERS/CALIBRATION SELECTOR	51
7.7	NETWORK AND REMOTE COMMUNICATION	51
7.8	RECEIVER SUB-SYSTEM DESIGNS PROVIDED BY INAF	51
8	SUMMARY OF RECEIVER MINIMUM REQUIREMENTS	52



UNIONE EUROPEA
Fondo Sociale Europeo
Fondo Europeo di Sviluppo Regionale



9 CONCLUSIONS	54
APPENDIX A: SRT SCIENCE WITH THE W-BAND MULTIBEAM RECEIVER.....	55
APPENDIX B: SRT OPTICS.....	57
APPENDIX C: SRT ATMOSPHERIC SITE CHARACTERIZATION AND MONITORING	61
APPENDIX D: W-BAND RECEIVER ARRAY ARCHITECTURES.....	64
APPENDIX E: SECOND DOWN-CONVERTER (FBCB) AND W-BAND RECEIVER OBSERVING MODES.....	65
E1. OBSERVING MODES FOR 3×3 2SB RECEIVER ARCHITECTURE	66
E2. OBSERVING MODES FOR 4×4 SSB RECEIVER ARCHITECTURE	68
REFERENCES	69



UNIONE EUROPEA
Fondo Sociale Europeo
Fondo Europeo di Sviluppo Regionale



1 Executive summary

The Sardinia Radio Telescope (SRT) is a new Italian facility for radio astronomy managed by INAF. The telescope is currently equipped with radio astronomy receivers covering the $\approx 0.3\text{--}26.5$ GHz frequency range. However, the SRT has been designed to operate with good efficiency up to a maximum frequency of ≈ 100 GHz ($\lambda = 3$ mm) with receivers to be installed at the Gregorian focus.

Here, we describe the top-level technical requirements of a 3 mm band (W-band) multibeam receiver based on a cryogenic focal plane array of dual-polarization feed-systems utilizing cryogenic low noise amplifiers (LNAs), which we aim at acquiring, installing and get operational on the Gregorian focus of the SRT. The array shall be designed to fit in the usable area of the focal plane and to provide optimum beam patterns with high antenna efficiency. This instrument will allow a significant technical and scientific upgrade of the SRT that will become one of the few single-dish radio telescopes in the world capable of carrying out high-sensitivity spectro-polarimetric astronomical observations across the 3 mm band, making of it an almost unique facility in the international context (see Appendix A). A W-band multibeam receiver on the SRT will fully justify the design and fabrication costs of the telescope, which were mainly determined by the technical specifications on accuracy of the primary and secondary reflectors.

INAF is going to procure the receiver through a "competitive dialogue", i.e. a co-engineering work with economic operators (institutions, companies or consortia) intending to bid for its development. Only proposals of construction of a full receiver (not of its sub-assemblies), complying with a minimum set of requirements, will be considered. During the competitive dialogue, whose regulations are described in the associated "OR1 Tender Document," INAF will interact individually with the tenderers (under Non-Disclosure Agreement) and will discuss the possible technical solutions to adopt for the receiver. These proposed solutions shall be technically sound and the claims fully supported by detailed analysis. The outcomes of the competitive dialogue will be used by INAF to prepare the final instrument specifications that will be adopted for the final tendering phase. Therefore, the detailed instrument technical specifications (like number of pixels, array configuration, down-conversion scheme, etc.) are not determined in the current phase, in order not to restrict possible solutions. The contract between INAF and the awarded supplier is expected to be signed within seven months from the date of publication of the present document. The receiver shall be finalized within the assigned timescale (approximately 21 months from contract signature to on-site acceptance test at the supplier laboratory) and budget (maximum net of VAT 2.3 M€).

INAF has already conducted an advanced feasibility study of the W-band multibeam receiver for the SRT, including the optics, the cryogenic modules, the Dewar, the mechanical derotator, the down-conversion system, etc. The baseline technical specifications of the instrument and the preliminary results of the INAF study were presented in document [1]. Some of the instrument baseline specifications were later revised and the revisions were presented at the "W-band multibeam receiver Information Day," held at INAF-Astronomical Observatory of Cagliari on Feb. 20th, 2019 [2].



UNIONE EUROPEA
Fondo Sociale Europeo
Fondo Europeo di Sviluppo Regionale



This document presents the updated baseline specification of the W-band multibeam receiver and the results of the INAF preliminary study; it is extracted from an INAF internal report under publication [3].

While some of the instrument technical specifications are already defined, as they are imposed by the electrical, mechanical and control software interfaces with the SRT telescope, others will be determined during the competitive dialogue.

Therefore, the goal of this document is three-fold: first, we provide a set of baseline specifications of the receiver and a list of more advanced architectures and configurations with increased complexity (and cost). Second, we include the result of the receiver advanced study carried out at INAF with preliminary 3D sketches of the instrument and of its sub-assemblies (Dewar, cryogenic modules, down-converter, mechanical derotator, etc.) in support of the work to be carried out by the interested economic operators. Third, we provide details of the hardware and of the monitor control software that must be adopted for the receiver in order to comply with the existing SRT telescope interfaces.

The array receiver will be based on a minimum of nine dual-linear polarization feeds in 3×3 configuration for the 75-116 GHz band capable of high-efficiency illumination of the antenna. The goal is an array of 16 feeds in 4×4 configuration for the 70-116 GHz band. The receiver shall be designed to provide high mapping efficiency by optimizing the geometry and the separation between the projected beams on the sky.

The dual linear polarization shall be achieved by means of dual-polarization feed-systems where each array element employs a cascade of corrugated feed-horn, OrthoMode Transducer (OMT) and HFET Low Noise Amplifiers (LNAs) cryogenically cooled at ≈15-20 K inside a cryostat.

Due to the shaped configuration of the SRT the usable focal plane area at the Gregorian focus is limited to feed-horns whose axis are placed within a radius of ≈65 mm from the telescope optical axis. To be confined within the ≈130 mm diameter, a 9-element dual-polarization focal plane array in 3×3 configuration can adopt a feed spacing of ≈45 mm, although shorter spacing would be desirable. Instead, a dual-polarization array in 4×4 configuration necessarily requires to design cryogenic modules with smaller footprint size where the feed spacing is ≈31 mm. The module would have to adopt OMT waveguide outputs/LNA inputs with non-standard miniaturized waveguide flanges.

The cryogenic modules shall provide a minimum of $9 \times 2 = 18$ waveguide outputs to a down-converter based on a tuneable Local Oscillator (LO) to be located at room temperature. The down-converter shall provide a minimum of 12 GHz band of Radio Frequency (RF) sky coverage (goal 16 GHz) for each of the two polarization channels. The two following architectures will be considered:

- a) a Sideband Separation down-converter (2SB) providing two independent Intermediate Frequency (IF) outputs (per polarization per feed), one resulting from the conversion of the USB (Upper Side Band), the other from the conversion of the LSB (Lower Side Band). Each sideband must have a total instantaneous bandwidth of at least 6 GHz (for example 4-10 GHz) with goal 8 GHz across 4-12 GHz (the value of the central IF frequency is not a specification).
- b) a Single Side Band (SSB) down-converter providing a single IF output at least

12 GHz wide (for example 4-16 GHz or 2-14 GHz), with goal 16 GHz across 2-18 GHz.

The down-converter could adopt either fundamental mixing or harmonic mixing schemes and shall include a LO distribution to the different pixels. In both cases (2SB or SSB), the 1IF frequency range (the prefix “1” refers to the 1st intermediate frequency down-conversion) of each sideband must fall across the 2-18 GHz range in order to be compatible with the subsequent processing hardware to be developed by INAF.

In case of option *a*), a receiver with nine dual-polarization elements would deliver at its down-converter output a total of 36×8 GHz-wide 1IF bands (9 feeds × 2 pols × 2 sidebands); in case of option *b*), a receiver with 16 dual-polarization elements would deliver at its downconverter outputs a total of 32×16 GHz-wide IF bands (16 feeds × 2 pols × 1 sideband). These first intermediate frequency 1IF signals will be transported to the 2-18 GHz second down-converter and to the following digital backend by means of the 38×20 GHz analogue optical links (RFoF20).

Additional multibeam configurations, with different pixel number (for example 3×4), and different 1IF output bands/schemes are possible and will be evaluated by the tender selection committee.

The receiver shall include a cabinet with racks for biasing all the cryogenic and room temperature active sub-systems, a mechanical derotator to maintain the parallactic angle during source tracking, a mechanical support structure for its permanent installation in the receiver cabin and a vacuum pump with remotely controlled vacuum valve.

Furthermore, the instrument must be capable of observing the Sun at 78 GHz and at 110 GHz (in two different receiver settings, not simultaneously) without saturating the receiver chain. Two solar band-pass filters (BPFs), with central frequencies at 78 GHz and 110 GHz, each with relative RF band of order 6%, could be adopted to reduce the signal power and mitigate the saturation problem. The solar filters could be switched in the signal path by a suitably designed switching mechanism, mounted in front of the vacuum window.

The receiver shall include a calibration system with at least one room-temperature (296 K) calibration load, which could also be mounted on the switching mechanism in front of the vacuum window. More complex calibration schemes will be considered, based for example on two loads - one cryogenic and one room temperature - on waveguide noise injection for the individual pixels, or on external noise-injection transmitter.

In the framework of an agreement between INAF and the Italian Space Agency (ASI) it is foreseen that the SRT will be equipped with transmitters operating in X-band and Ka-band for spacecraft communication (Sardinia Deep Space Antenna). Therefore, all receivers and equipment to be installed near the SRT transmitters beam propagation path, including the W-band multibeam receiver, might potentially be exposed to electromagnetic fields of significant intensity when the telescope is operated in transmission mode. At the moment, it is not possible to foresee the exact power levels and electromagnetic environment at which the receiver will be exposed. For this reason, if possible without performance degradation and delay on the delivery time, it is requested that the W-band receiver be designed for maximum protection from strong X-band and Ka-band signals in all its sensitive parts. In all cases, whether proper shields are applied or not, it is requested that the supplier provides

the maximum tolerability threshold of the various receiver components to allow INAF and ASI to prepare appropriate countermeasures to preserve their integrity and performance.

The W-band receiver shall be free from self-generated Radio Frequency Interference (RFI) in order not to contaminate the environment during radio-astronomy observations with other receivers. The receiver must include all sub-systems up to the output of the 11F cable wrap (part of the derotator mechanism, cascaded to the first down-converter). The second down-conversion and the subsequent receiver stages will be developed by INAF and have not to be supplied.

The receiver shall be fully characterised in the laboratory of the supplier and shall comply with the specification before its shipping to the SRT site (on-site factory acceptance test by end of December 2021). The receiver shall be provided along with a series of spares of its most critical parts, including LNAs and down-converter modules. Also, an “user manual” for the instrument with step-by-step operation procedure shall be provided. The manual shall include the characterization results with compliance datasheet of the instrument.

The receiver shall be installed on the rotating platform of the SRT Gregorian focus with the technical support of INAF personnel. The preliminary receiver acceptance test on telescope shall be carried out by the supplier by mid-February 2022, before the instrument is released for full technical and scientific commissioning to the INAF team.

The estimated timeframe for developing the instrument, delivering it to SRT and its pre-commissioning on the telescope is estimated to be of order 22 months following the signature of the contract with the company/consortium. The project, including the financial closure, shall be completed by the 24th of February 2022.

The contract will be awarded, following the rules described in the OR1 Tenderer Document. The main technical selection criteria for the W-band receiver will be based on the proposed number of pixels, antenna efficiency for off-axis beams, beams separation, RF and IF bandwidths, receiver noise temperature and image rejection ratio.

2 Introduction to SRT

The SRT is a new Italian radio telescope designed for scientific radio astronomy application. It operates in single-dish (continuum, full Stokes and spectroscopy), Very Long Baseline Interferometry (VLBI) and Space Science modes. The telescope is a fully steerable wheel-and-track dish (Figs. 1 and 2), 64-m in diameter, located 35 km north of Cagliari, on the island of Sardinia, Italy. The SRT optical design is based on a quasi-Gregorian configuration (Fig. 3) with shaped 64-m diameter primary (M1) and 7.9 m diameter secondary (M2) reflectors to minimize spillover and standing waves.

The 64-m primary mirror can be constantly adjusted in quasi real-time by electromechanical actuators with the aid of a metrology system, allowing for the correction of both the systematic effects due to gravity and the non-systematic effects due to wind and thermal variations. The active primary reflector will allow to achieve a surface accuracy of about 150 μm (RMS, compared to the ideal profile) corresponding to about $\lambda/20$ in W-band. An extensive atmospheric study at the SRT site indicates that it will be possible to carry out



UNIONE EUROPEA
Fondo Sociale Europeo
Fondo Europeo di Sviluppo Regionale



radio astronomy observations across the 3 mm bandwidth for a good fraction of time during the winter seasons.

The telescope is designed to host up to twenty receivers installed in six focal positions: Primary focus (F1), Gregorian focus (F2) and Beam-Wave Guide foci (F3&F4 and F5&F6), respectively with focal length to diameter ratio (F/D) and frequency ranges equal to 0.33 (0.3-20 GHz), 2.34 (7.5-116 GHz), and 1.38 & 2.81 (1.4- 35 GHz). The W-band multibeam receiver shall be installed at the Gregorian focus F2.

Figure 3 and Table 1 show the main optical specifications of the SRT. The f-ratio at the Gregorian focus, where the 3 mm multibeam receiver shall be installed, is $f_2/D \approx 2.34$ (see also Appendix B). The angle subtended by the edge of the sub-reflector with respect to the optical axis, as seen from the Gregorian focus, is 12 deg.

The telescope aims at driving numerous important discoveries and transforming our understanding of the Universe. Its formal inauguration took place in September 2013. Following a six-month Early Science Program carried out in 2016 and a refurbishment of its active surface, the antenna has been open for scientific observation to the international community since December 2018 and is delivering world-class scientific results (see http://www.srt.inaf.it/astonomers/science_srt/).

Further SRT details can be found at the following web page: <http://www.srt.inaf.it/>

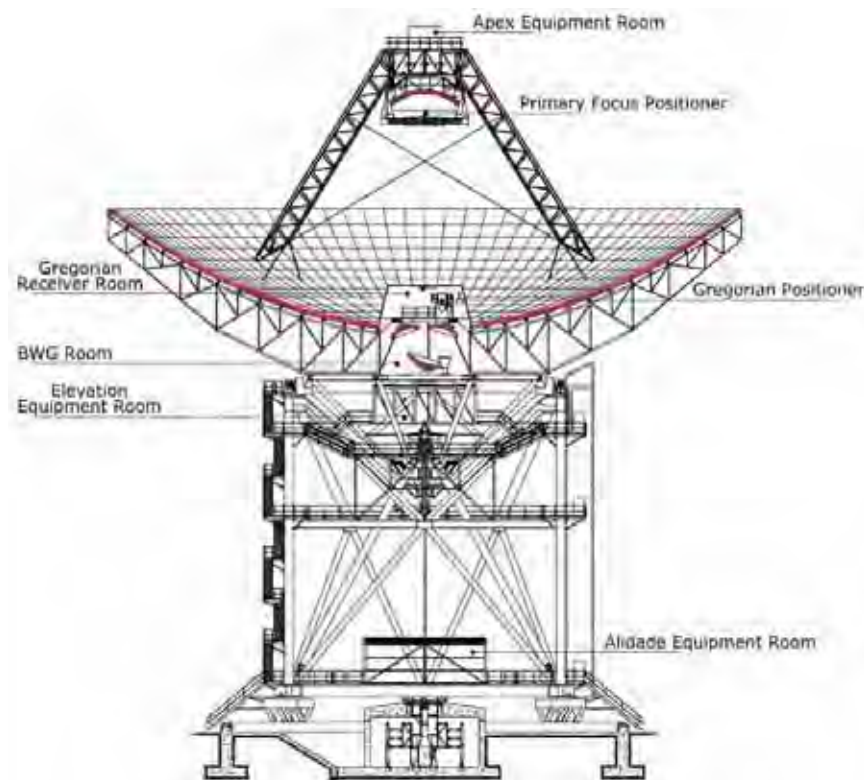


Fig. 1. Cross-cut of the 64-m diameter Sardinia Radio Telescope (SRT) outlining the main reflecting surfaces (in red).



UNIONE EUROPEA
Fondo Sociale Europeo
Fondo Europeo di Sviluppo Regionale



Fig. 2. Photo of the SRT, located in the municipality of San Basilio, Sardinia island, Italy.

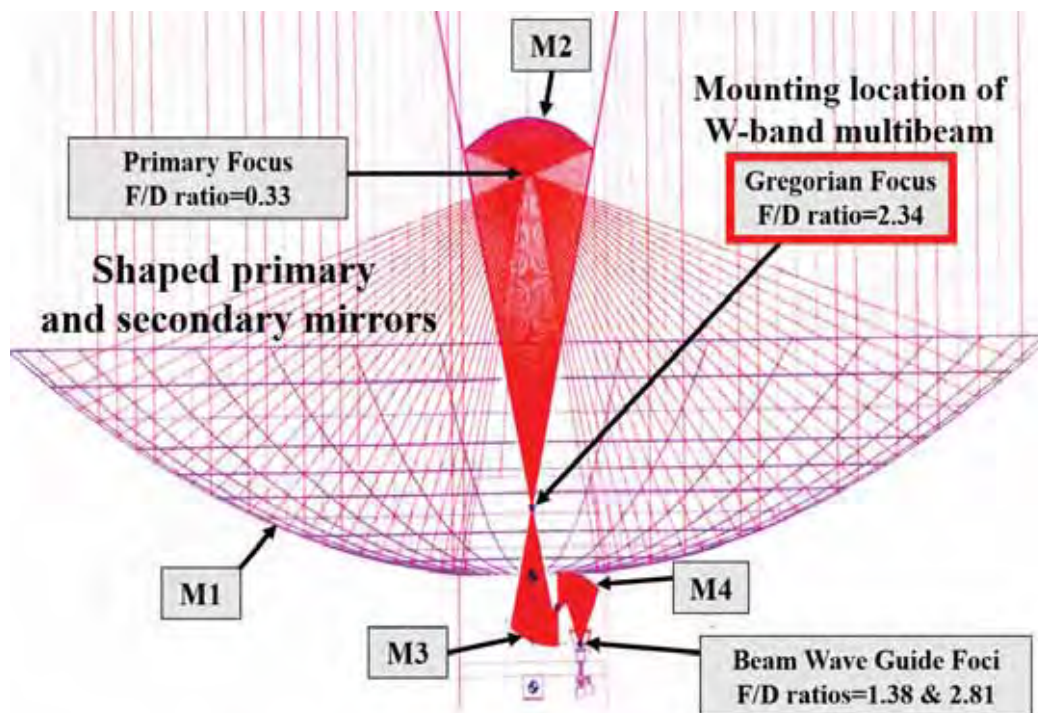


Fig. 3. Optical configuration and ray tracing of the Sardinia Radio Telescope showing the 64-m diameter primary (M1), the 7.9-m secondary (M2), and two additional Beam Waveguide (BWG) mirrors (M3 and M4). Three out of six possible focal positions (primary, Gregorian and BWG) are shown together with corresponding focal ratios. The mounting location of the W-band receiver is at the Gregorian focus ($f/D=2.34$).



<i>Optical configuration</i>	Shaped Gregorian
<i>Sub reflector geometry</i>	Numerical
<i>Prime mirror diameter, D [m]</i>	64.008
<i>Sub reflector diameter, d [m]</i>	7.9060
<i>Focal length, f [m]</i>	21.0236
<i>Prime focus focal ratio, f_1/D</i>	0.3285
<i>Secondary focus focal ratio, f_2/D</i>	2.342
<i>Distance from Prime to Gregorian foci [m]</i>	17.4676
<i>Magnification, M [m]</i>	7.13
<i>Prime focus to sub reflector vertex [m]</i>	2.8524
<i>Secondary focus to sub reflector vertex [m]</i>	20.3200
<i>Secondary focus to primary mirror vertex [m]</i>	3.5560
<i>Distance from Prime mirror vertex to aperture plane [m]</i>	12.1415
<i>Distance from Prime focus to aperture plane [m]</i>	8.8821
<i>Prime mirror half-angle [degree]</i>	74
<i>Sub-reflector half-angle [degree]</i>	12

Table 1. Optical parameters of the Sardinia Radio Telescope.

3 W-band receiver architecture: noise and image band rejection

The minimum system noise temperature of a heterodyne receiver is set by the quantum limit, $T_{\min} = h\nu/k_B \approx 5$ K at 100 GHz, where $h = 6.62 \times 10^{-34}$ J·s and $k_B = 1.38 \times 10^{-23}$ J/K are, respectively Planck's and Boltzmann's constants. Heterodyne receivers with state-of-the-art performance achieve noise temperatures of few times the quantum limit across W-band, of order 30 K ($6 \times T_{\min}$), when the noise is referred to the receiver input. In a practical implementation on a telescope, the losses associated with infrared filtering, local oscillator (LO) injection, telescope spillover and atmospheric attenuation all contribute to degrade the actual figure of merit for astronomical spectroscopy: the SSB system noise temperature T_{SSB} , where all the noise is referred to the signal input. In particular, the atmospheric noise entering the receiver in the image sideband can considerably impact the overall system noise and degrade the ultimate instrument sensitivity, unless the image sideband is rejected. Appendix C provides some results of the analysis of the SRT atmospheric site with estimated system noise temperature and fraction of the useful observing time across the 3 mm band atmospheric window.

In the case of sideband separating (2SB) receivers, the upper (USB) and lower (LSB) sideband frequencies, respectively $\nu_{\text{USB}} = \nu_{\text{LO}} + \nu_{\text{IF}}$ and $\nu_{\text{LSB}} = \nu_{\text{LO}} - \nu_{\text{IF}}$, are down-converted to two independent Intermediate Frequency IF outputs as depicted in Fig. 4. Here, ν_{LO} and ν_{IF} indicate, respectively the LO and IF frequencies and it is assumed that there is no conversion from higher harmonic sidebands. The conversion power gains from each RF input port to each IF output of the 2SB receiver is denoted by the quantities $G_{i,j}$. The image rejection ratios R_i are the ratio between the following USB and LSB gains:

$$R_1 = G_{1U}/G_{1L} \text{ at IF port 1}$$

$$R_2 = G_{2L}/G_{2U} \text{ at IF port 2}$$

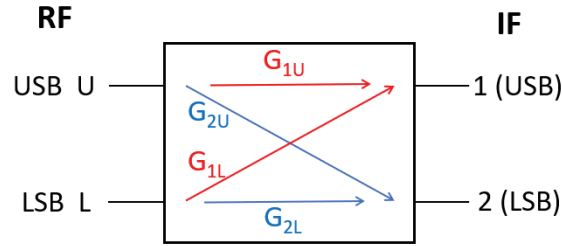


Fig. 4. Power gains of a sideband separating receiver. The upper (USB) and lower (LSB) sideband ports are normally the same waveguide or transmission line, but are shown separately here for clarity.

The image sideband rejection is infinite in the ideal case but may be as low as 10 dB in practice. For a double sideband (DSB) receiver, the sideband ratio is unity, and the receiver has no rejection (0 dB).

We note that the sideband ratios of interest in radio astronomy ($R_1 = G_{1U}/G_{1L}$ and $R_2 = G_{2U}/G_{2L}$) depend on the gain flatness of the RF components in front of the sideband separating mixer adopted for sideband rejection (unlike the gain ratios G_{1U}/G_{2U} and G_{2L}/G_{1L}) so that the passive components and low noise amplification chains in front of the downconverter should ideally have a flat response.

The single side band (SSB) noise temperature of a heterodyne receiver with sideband ratio R_i ($0 \leq R_i \leq \infty$), is obtained by correcting the measured double side band (DSB) noise temperature for the image contribution to the IF output

$$T_{R,SSB} = T_{R,DSB}(1 + 1/R_i) \quad (1)$$

Thus, unless the sideband ratio is very high (for example $R_i > 100$ in linear scale, equivalent to >20 dB) a correction is required for a precise evaluation of the single-sideband receiver noise temperature, deduced from the Y-factor measurement using broadband hot and cold loads.

The W-band multibeam receiver for the SRT Gregorian focus shall be equipped with cryogenic LNAs delivering ultra-low noise performance and shall adopt a down-conversion scheme that achieves a signal-to-image sideband gain ratio $R_i > 10$ dB at all frequencies.

The image rejection reduces the noise contribution entering the receiver in the image sideband (including the atmospheric noise)². This decreases the overall system noise and reduces by the factor R_i the contamination of spurious lines observed at the first intermediate frequency 1IF signals from the unwanted sideband.

The SSB receiver noise temperature of all dual-polarization pixels of the W-band multibeam for SRT is expected not to exceed $T_{R,SSB} = 70$ K full band. The noise shall be corrected for true single side band response, i.e. corrected for the residual image response according to Eq. 1, and account for the noise contributions from the Dewar vacuum window,

² When the noise is dominated by the atmospheric contribution, rather than by the receiver noise itself, a receiver with very high image rejection ratio ($\gg 1$) delivers half the SSB system noise temperature of one with no rejection (i.e. with signal-to-image sideband 0 dB, with equal gains in the image and in the signal bands).

the IR filter, the feed, the OMT, the LNAs, the down-converter and all the noise contributions up to the receiver Intermediate Frequency output ports.

The receiver can adopt different architectures in terms of pixel number, down-conversion scheme, instantaneous 1IF band, placement of components inside or outside the cryostat, etc.

Figure 5 shows one of the possible architectures based on a 3x3 focal plane array, where a cascade of feeds, OMTs and LNAs covering the 75-116 GHz band are cryogenically cooled at $\approx 15-20$ K inside a cryostat. Here, 18 band pass filters (BPFs) and down-converters (three modules of three-pixel down-converters) based on sideband separating scheme are cascaded to the cryostat components and located at room temperature along with a local oscillator distribution system. The focal plane array (cryostat and down-converters) must be mechanically de-rotated to track the parallactic angle during source tracking. The two 4-12 GHz 1IF (first intermediate frequency) signals for each of the two polarization channels of each pixel are transported by 36 coaxial cables (≈ 4 m long) through the derotator 1IF cable wrap up to the input of the 1IF switch matrix.

A detailed description of the receiver elements and of alternative architectures is provided in the following sections.

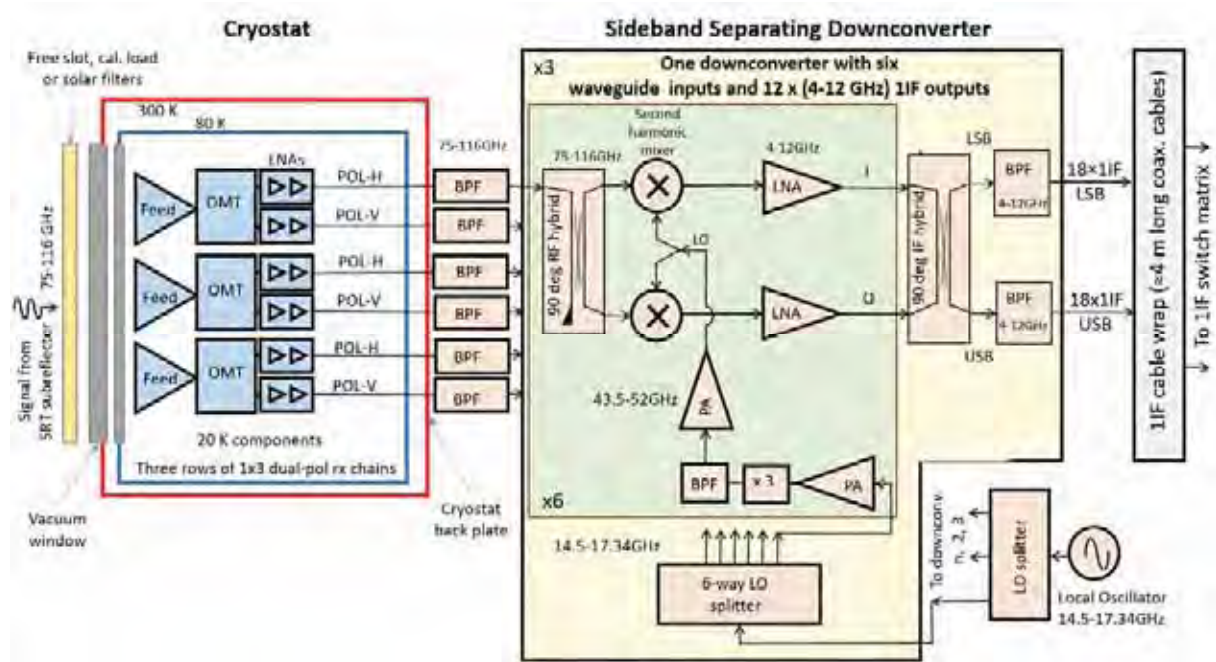


Fig. 5. Possible W-band multibeam receiver architecture in 3x3 configuration covering 75-116 GHz showing the cryogenic components and the room temperature sideband separating down-converters delivering 36x1IF outputs (18xUSB and 18xLSB) across 4-12 GHz. The down-converters could consist of three independent modules, each serving a line of three dual-polarization cryogenic pixels. The 1IF (first down-conversion) signals are transported by coaxial cables from the down-converter to the 1IF switch matrix (not part of the receiver). The receiver shall include a mechanical derotator (not shown).

4 Mounting of the array receiver at the SRT Gregorian focus

In this section we present the mounting location and arrangement of the W-band receiver.

4.1 GREGORIAN FOCUS RECEIVER POSITIONER

Figure 6 shows a 3D view of the Gregorian and Beam Waveguide focal points and the location where the W-band multibeam receiver shall be mounted along with its mechanical support frame. The instrument shall be located on the Gregorian focus receiver positioner (GRP), a rotating platform eccentrically mounted in the Gregorian focal plane. Images of this rotating platform, showing also a preliminary design concept of the W-band receiver, are shown in Figs. 7-8. The GRP has a decagonal shape and will host up to eight cryogenic receivers for operation over a range of frequencies from 4.2 GHz to 116 GHz. A drive system can rotate the turret so that any of the receivers can be positioned on the optical axis of the telescope.

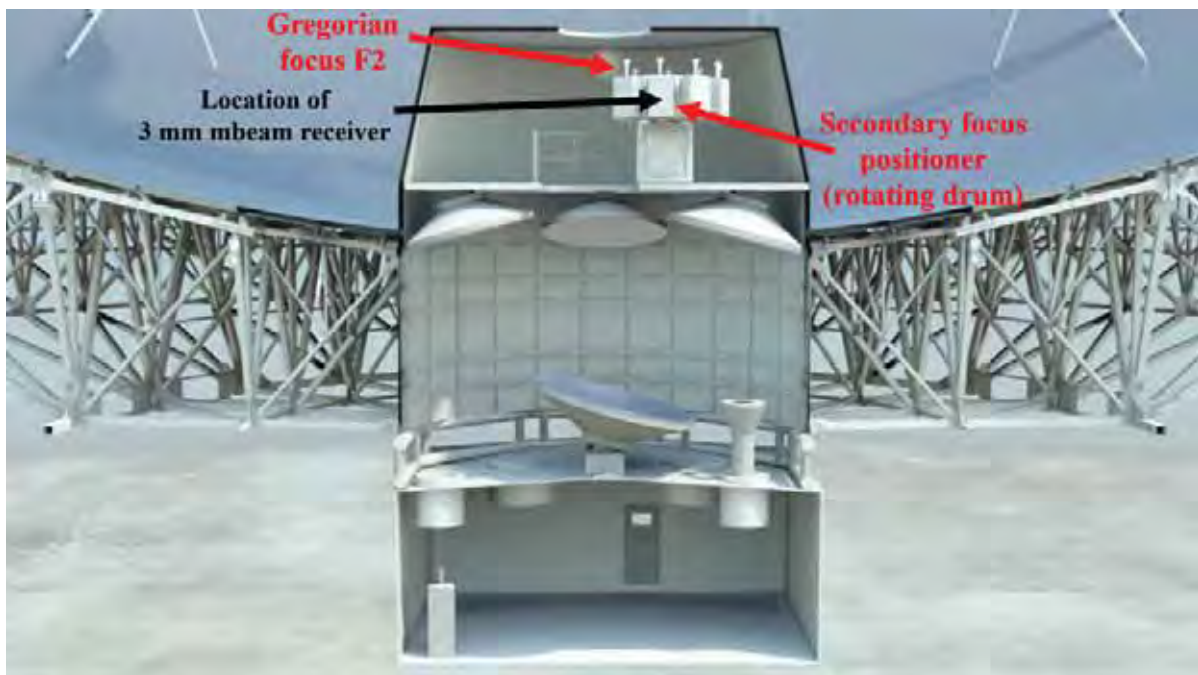


Fig.6. Gregorian and Beam Waveguide receiver cabins. The W-band (3 mm band) multibeam receiver shall be installed on the Gregorian receiver positioner (rotating drum).



UNIONE EUROPEA
Fondo Sociale Europeo
Fondo Europeo di Sviluppo Regionale

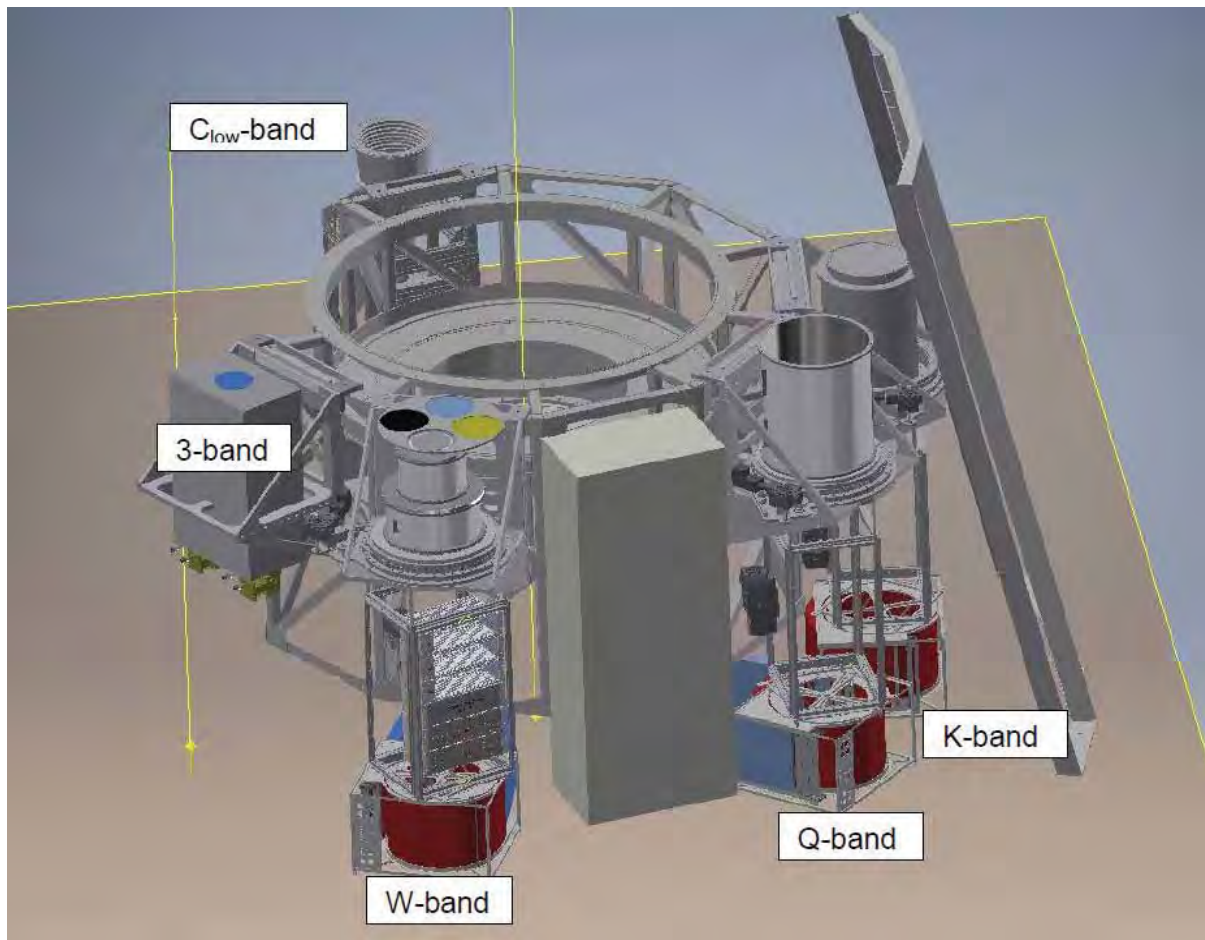


Fig.7. View of the Gregorian receiver positioner showing a preliminary design of the W-band multibeam receiver (W-band) and of the other front-ends that will be available at the Gregorian focus (F2): Q-band, K-band, 3-band, C-low band. A bolometric camera (not shown) will also be installed on the GRP.

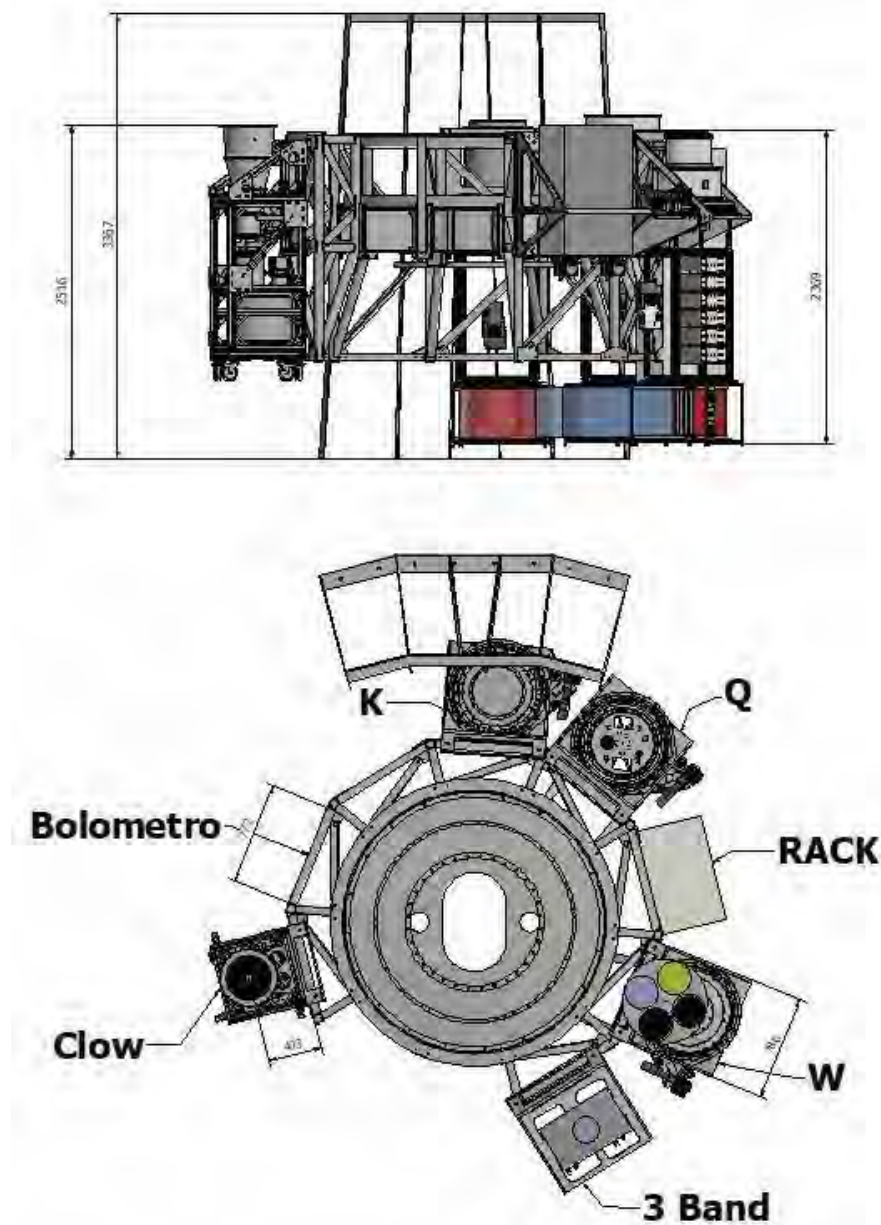


Fig.8. Lateral view (top panel) and top view (bottom panel) of the GRP showing the future arrangement of the receivers. The W-band multibeam receiver (indicated with W) is located between the "Rack" and the "3 Band" receiver. Dimensions are in mm.

The maximum dimensions of the W-band receiver in the vertical direction (parallel to the optical axis) is 2465 mm and its maximum weight (including mechanical support frame, derotator, racks with electronics, etc.) is 250 kg. The size and weight of the instrument are expected to be similar to the Gregorian focus K-band receiver developed by INAF [4], whose main dimensions and photo are shown in Fig. 9.

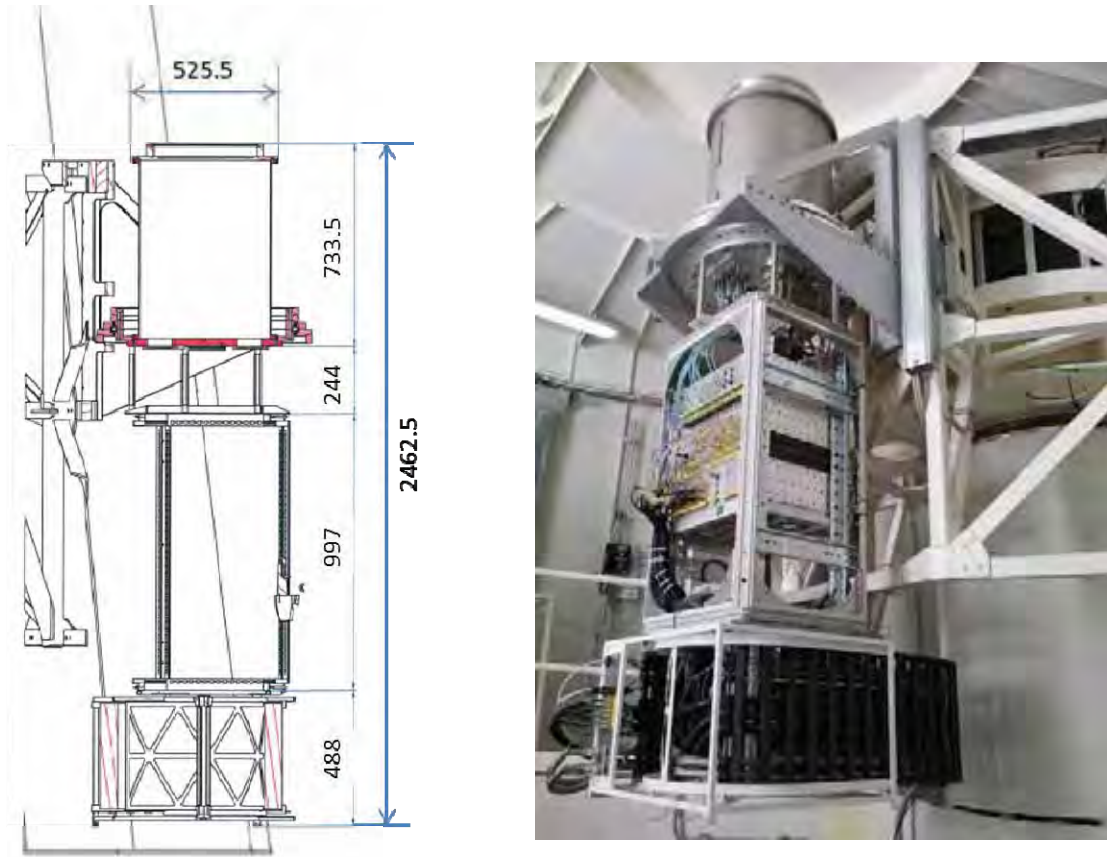


Fig. 9. K-band multibeam receiver installed on the SRT GRP: Side view with main dimensions (left panel) and photo of the receiver (right panel). From top to bottom: Dewar with derotator, electronics racks cabinet (down-converters, cryogenic control, etc.) and cable wrap. Dimensions are in mm.

4.2 MECHANICAL DEROTATOR AND CABLE WRAP

The W-band receiver shall include a mechanical derotator for tracking the parallactic angle during source tracking. Such derotator shall be compatible with the existing and future interfaces and control software that will be available on the antenna and it will be similar to the one used for the K-band receiver. Identical derotators are also planned for the Q-band Gregorian focus and for the S-band primary focus SRT multibeam receivers. Figure 10 shows some of the details of the K-band receiver cable wrap, which includes the flexible IF coaxial cables and the cryo-cooling helium flex lines. The cable wrap allows to guide the wrapping of cables and lines during the movement of the mechanical derotator around its axis. The derotator system, with its electro-mechanical parts, shall be supplied along with the W-band receiver, by the tenderer awarded company/consortium. The derotator shall be constructed according to the executive drawings that will be provided by INAF. Figure 11 shows two pictures of the rotating platform³. Additional details are provided in Section 6.

³ Additional three-dimensional drawings and pictures of the SRT receiver cabin can be found at the following link: https://drive.google.com/drive/folders/1WkPPg4mKO2eieX1Az4zo6qSFeC_egQ5r?usp=sharing



UNIONE EUROPEA
Fondo Sociale Europeo
Fondo Europeo di Sviluppo Regionale



Fig. 10. Photos of the cable wrap of the K-band multibeam receiver.



Fig. 11. Photo of the rotating platform supporting the receiver(s), with K-band receiver off the focal plane (top panels) and on the focal plane (bottom panel).

5 Optical configuration and cryogenic modules

The W-band array receiver shall be designed for high-efficiency illumination of the SRT dish with low sidelobes, low cross-polarization level and high beam circularity for both the on-axis and off-axis feeds. The receiver shall also be designed to provide high mapping efficiency by optimizing the geometry and the separation between the projected beams on the sky. For large-area mapping purposes it would be desirable to achieve the smallest possible separation between the projected beams, compatibly with high-efficiency dish illumination corresponding to a minimum $2 \times \text{HPBW}$ (Half Power Beam Width), where HPBW is wavelength and illumination dependent and of order $1.22 \lambda/D$, with $D=64$ m. For $\lambda=3\text{mm}$ ($\nu=100$ GHz), $\text{HPBW} \approx 11$ arcsec. The ratio between beam spacing and HPBW must be in the range 2 to 5.5 at all frequencies across the 70-116 GHz band of the W-band receiver. The

specification on the maximum value of this ratio, 5.5, is set by considerations on mapping efficiency of radio astronomy sources that are not too extended and on the maximum number of on-the-fly (OTF) sub-scans required to cover a given region of the sky (see also Appendix B).

Different receiver architectures and cryogenic array configuration can be adopted to achieve the required high-efficiency SRT illumination and beam spacing, including the following:

- re-imaging optics in front of the array;
- non-modular array designs (for example in platelet);
- modular designs based on dual-polarization feed systems with OMTs, each cascaded with two independent LNA chains or with a single dual-polarization LNA chain;
- modular designs based on dual polarization feed system with cryogenic “active OMT” that integrates LNAs;

Below, we present the results of the INAF preliminary design study of some possible W-band array configurations based on modular designs that do not require re-imaging optics. We illustrate possible examples of different cryogenic arrays solutions and set the constraints in terms of physical footprint size of each of the receiver modules.

5.1 SIZE OF FOCAL PLANE AT THE GREGORIAN FOCUS

The shaping of the SRT primary and secondary surfaces limits the telescope field of view (FoV) achievable from the Gregorian focus. We carried out electromagnetic simulations of the SRT radiation pattern and of the antenna efficiency by illuminating the telescope shaped optics (combination of secondary and primary mirrors) with a corrugated feed-horn located at the Gregorian focus [5]-[6]. Figure 12 shows the results of the electromagnetic simulations for the SRT antenna efficiencies calculated at 22 GHz and at 100 GHz as a function of the linear shift of the feed on the focal plane, expressed in wavelengths, with respect to the on-axis feed. The purple curve, referring to the illuminating feed at 100 GHz, shows that to maintain high antenna efficiency ($\approx 90\%$ of the on-axis feed, equivalent to -0.5 dB loss), the maximum offset of the feed must be less than $\approx 21\lambda$, corresponding to a maximum linear displacement on the focal plane of approximately ≈ 63 mm (at 100 GHz). The maximum drop of efficiency that could be tolerated at any frequency across 70-116 GHz is $\approx 20\%$ of the on-axis feed (equivalent to $\approx 80\%$ of the on-axis efficiency, or -1 dB loss). An $\approx 80\%$ antenna efficiency is achieved at all frequencies by confining the cluster of corrugated feed-horns within a radius of ≈ 65 mm from the telescope axis (restriction from the upper frequency edge 116 GHz, see Appendix B). Therefore, the diameter of the SRT Gregorian focal plane for high-efficiency illumination at ≈ 3 mm is of order 130 mm.

5.2 FEED-SYSTEM (SINGLE CHAIN)

The radiating feeds must be designed to provide high-efficiency illumination of the SRT antenna at 12 deg half-angle ($f_2/D=2.34$) across 70-116 GHz (75-116 GHz). The edge taper should be ≈ 12 dB at 93 GHz (central frequency).

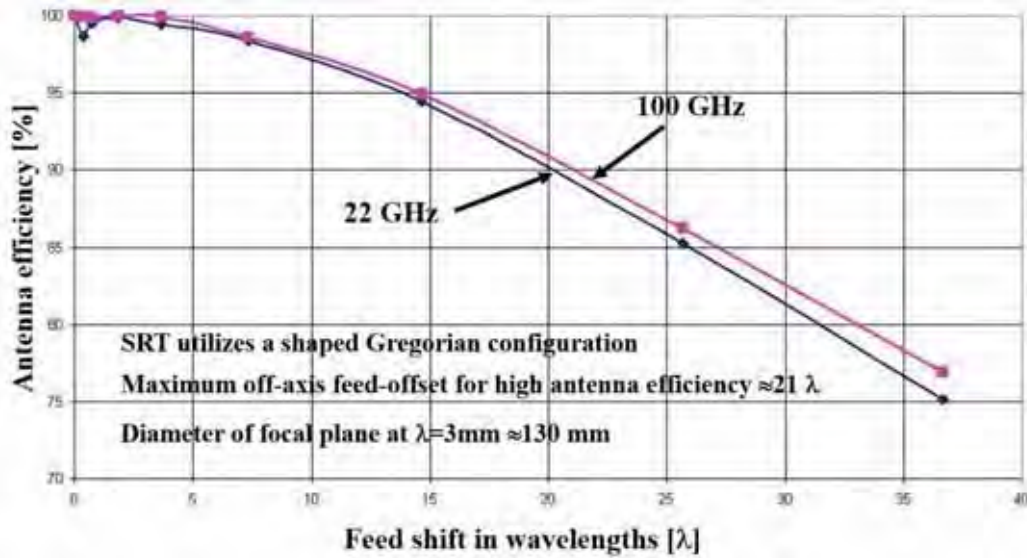


Fig. 12. Simulated antenna efficiency at 22 GHz and at 100 GHz when the SRT is illuminated from the secondary (Gregorian) focus versus feed offset from the on-axis feed. The offset on the focal plane (orthogonal to the optical axis) are expressed in wavelengths ($\lambda=3$ mm for $\nu=100$ GHz).

In the past years INAF successfully developed prototypes of feed-horns and OMTs [6] for the ALMA Band 2+3 (67-116 GHz) receiver cartridge funded by ESO in the framework of the “Advanced Study for the Upgrades of the ALMA”. Such passive components are based on platelet design and are fabricated by electroforming techniques. The ALMA Band2+3 feed prototype has been modified and re-optimized for illumination of the SRT optics and for its potential use in the W-band focal plane array.

Figure 13 shows a 3D drawing of the original ALMA Band 2+3 feed-horn and OMT prototypes cascaded with four independent commercial low noise amplification modules (two per polarization channel). In the configuration shown in Fig. 13, the LNAs are

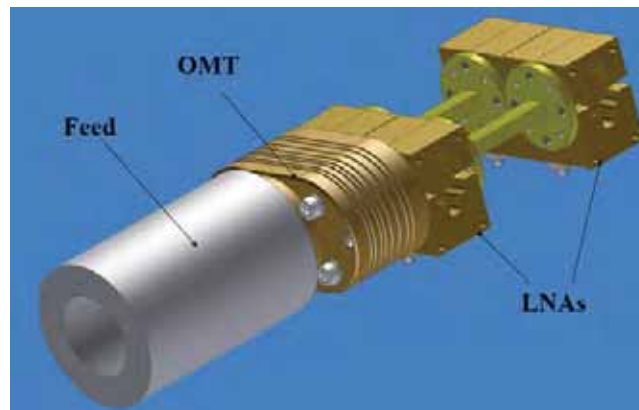


Fig. 13. 3D sketch of W-band single-pixel dual-polarization feed-system: cryogenic receiver chain (components cooled at ≈ 15 -20 K) showing the ALMA Band 2+3 feed-horn and OMT prototypes and two cryogenic LNA modules per polarization channel (total gain $G \approx 45$ dB). The LNA modules (each with gain $G \approx 23$ dB) are interconnected through a short section of waveguide with standard UG387 flange.

interconnected through a short section of WR10 waveguide with standard UG387 flanges. However, the final architecture of the cryogenic receiving chain might adopt different configurations, for example employing:

- 1) an isolator in place of the short waveguide section (to decrease the standing waves and improve matching);
- 2) a direct cascade of the two LNA modules with no interconnecting waveguides;
- 3) a second stage high-IP1dB LNA at room temperature (rather than two cryogenic LNA modules);
- 4) a single cryogenic LNA module for each polarization channel (gain ≈ 45 dB), rather than a cascade of two LNA stages (each with gain ≈ 23 dB);
- 5) a single LNA module for both polarization channels in cascade to the OMT (dual-polarization LNA);
- 6) an “active OMT” that incorporate LNAs in a dual polarization module;
- 7) any other possible solution that delivers the receiver specifications.

5.3 BASELINE W-BAND 3×3 RECEIVER ARRAY CONFIGURATION

The simplest configuration of the array would consist of nine dual-linear polarization feed horns arranged in a square 3×3 configuration like the one shown in Fig. 14. The feed-array could be placed either on the Gregorian focus or illuminate the dish through a suitable re-imaging optics. If placed at the Gregorian focus, this simple configuration with ≈ 45 mm feed separation cannot achieve the minimum beam spacing in the sky of $2 \times \text{HPBW}$. The dashed circle on Fig. 14 indicates the points on the Gregorian focal plane where the antenna gain is -0.6 dB below the on-axis gain at 100 GHz. The radius of circular FoV on the focal plane corresponding to this loss is approximately 21λ (≈ 63 mm at $\lambda \approx 3$ mm). The projection of the beams on the sky for the simple 3×3 optical configuration is also shown on Fig. 14. The beam separation is frequency-independent and equal to ≈ 62 arcsec, corresponding to $5.3 \times \text{HPBW}$ at 116 GHz, where $\text{HPBW} \approx 11.6$ arcsec, and to $4 \times \text{HPBW}$ at 70 GHz, where $\text{HPBW} = 15.2$ arcsec. The maximum acceptable value for the ratio beam-spacing/HPBW has been estimated to be about 5.5 at all frequencies.

Appendix B provides additional details on the optical design and illustrates the results of some preliminary electromagnetic simulations of such optical system carried out with the Grasp software using a 3×3 configuration. The degradation of the antenna efficiency obtainable for the four feeds placed at the vertices of the square configuration (n. 3, 5, 7, 9) is $\approx 18\%$ at 116 GHz and $\approx 5\%$ at 70 GHz with respect to the on-axis feed (n. 1). Such optical configuration would allow Nyquist mapping of large-scale astronomy fields with three passes using suitable scanning techniques.

An array consisting of 3×3 feeds with spacing between contiguous horns of ≈ 45 mm can fit inside the ≈ 63 mm FoV radius.

Views of one possible configuration of the 3×3 cryogenic array, with feed spacing corresponding to the illustration of Fig. 14, are shown in Figs. 15-16. The 3D sketches utilize the ALMA Band 2+3 feed-horn and OMT designs. A feed spacing of ≈ 45 mm allows to accommodate two UG387 waveguide flanges side by side (alignment pins and screw holes of

one such flange are located on a 19.05 mm diameter).

Although a 3×3 array with standard waveguide flanges could fit into a ≈ 130 mm diameter footprint it is desirable to reduce the feed spacing below ≈ 45 mm to achieve very high antenna efficiency of the off-axis beams and decrease the beam spacing in the sky.

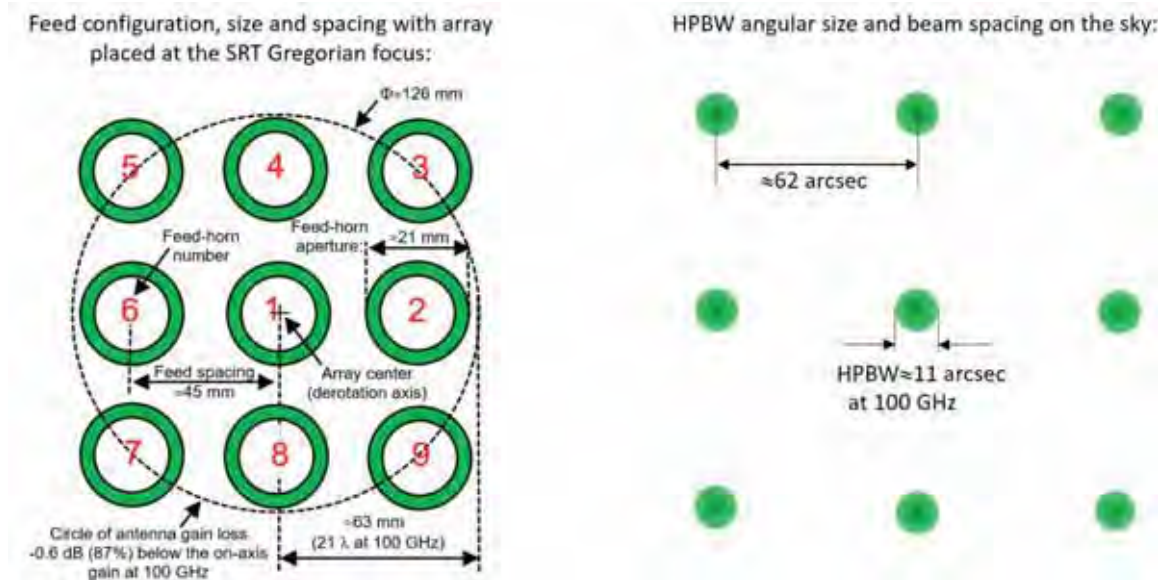


Fig. 14. Configuration of the array of 3×3 feeds on the Gregorian focal plane (left) and corresponding beams projected on the sky (right). The example refers to an array of feeds placed on the Gregorian focus without reimaging optics.

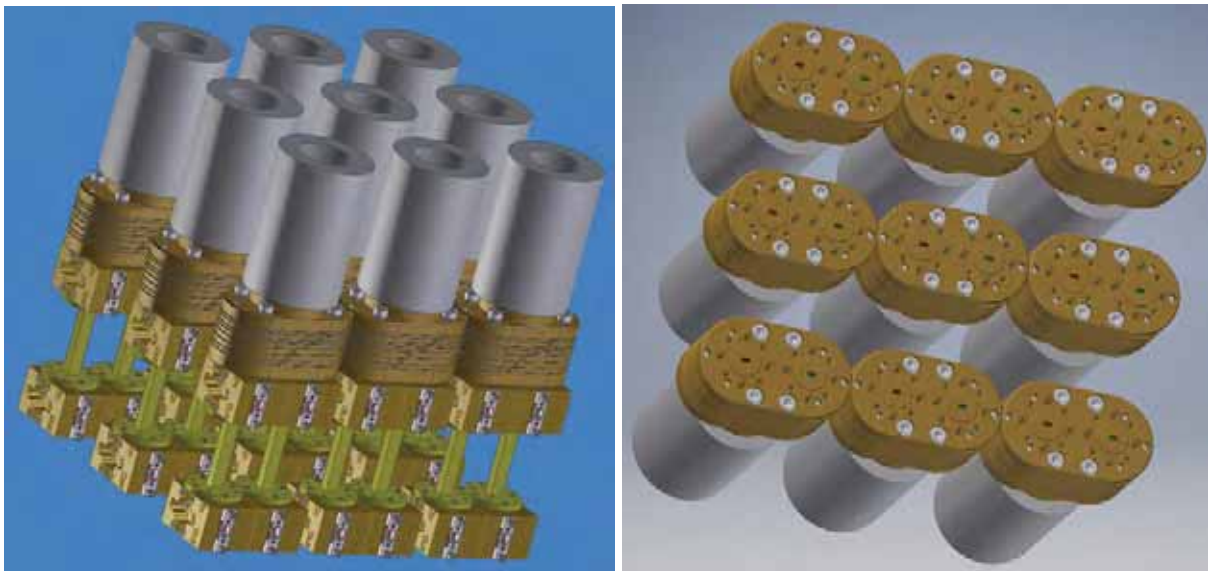


Fig. 15. Sketch of 3×3 cryogenic array based on the ALMA Band 2+3 chain: view of fully assembled array with feed+OMT+LNA modules (left panel). View of feed+OMT assembly showing the OMT output (right panel).

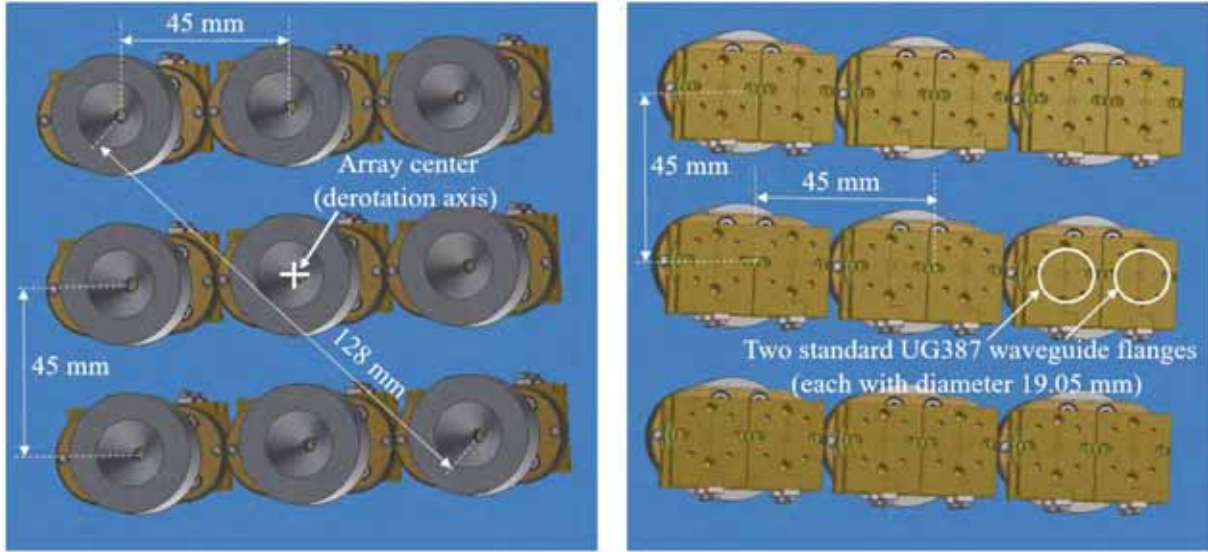


Fig. 16. Front view (left panel) and back view (right panel) of 3×3 W-band dual-cryogenic receiver array showing respectively the feed-horn apertures and the 18 (9 pixels × 2 polarizations) waveguide outputs of the LNA modules.

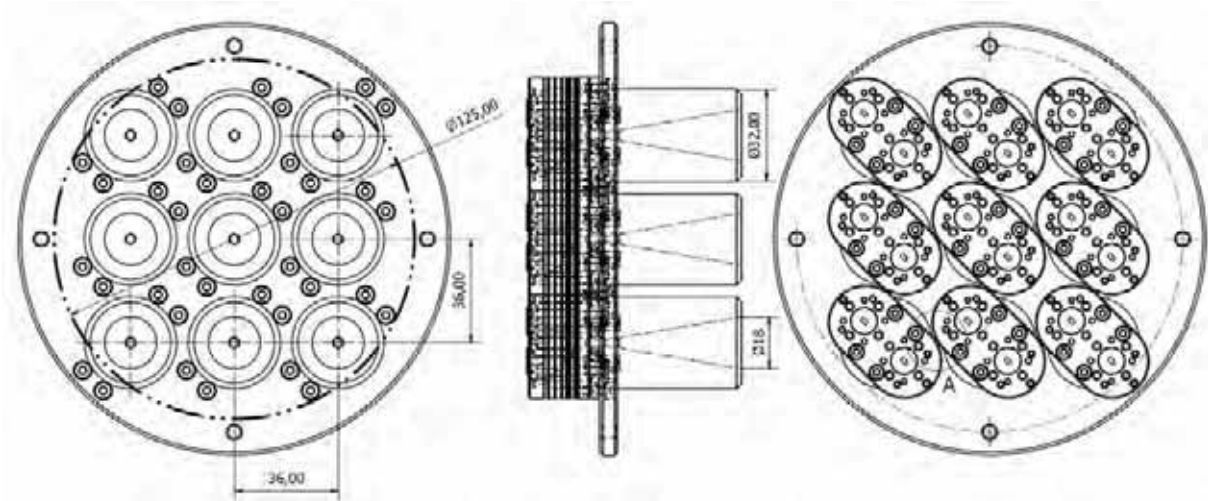


Fig. 17. Possible arrangement of the array based on feed cascaded with ALMA Band 2+3 OMT design.

Figure 17 shows an example of a different arrangement of a 3×3 array consisting of the same INAF feed-horn and OMT combination based on ALMA Band 2+3 designs, this time oriented at 45 degrees to the horizontal plane. This results in feed-horn inter-axis of 36 mm (axis of feed-horns confined within ≈ 102 mm). This arrangement is suitable for implementing the passive parts (feed and OMT) but requires development of non-commercial LNA module(s) with suitable footprint to fit behind them.

We carried out a preliminary feasibility study that indicates that a cryogenic dual polarization feed-system (feed, OMT and LNA) could be developed to fit into a spacing of order ≈ 31 mm without too significant development effort. The corresponding angular separation on the sky between contiguous beams would be ≈ 43 arcsec, i.e. about $3.7 \times \text{HPBW}$

at 116 GHz and about $2.8 \times \text{HPBW}$ at 70 GHz. The miniaturized cryogenic module should be based on non-standard waveguide flanges to allow the 9-element dual-polarization array to be confined into a small focal plane area of radius ≈ 44 mm ($\approx 15 \lambda$ at $\nu=100$ GHz), resulting in 95% antenna efficiency for the most offset feeds (Fig. 12).

Starting from the experience acquired in the ALMA Band 2+3 developments, INAF has designed a feed-horn and an OMT with small footprint, which would be suitable for integration in the W-band focal plane array for the SRT. The feed-horn provides high-efficiency illumination of the SRT from the Gregorian focus across the 70-116 GHz frequency band. The plots in Fig. 19 show the beam waist radius as a function of the distance from the feed-horn aperture at 78 and 107 GHz (the beam radius is the $1/e$ amplitude of the best-fit Gaussian beam). These values can be used to estimate the clearance diameter of all apertures in front of the feed-horns. Typically, the clearance diameter of all optical elements of the receiver (IR filter, vacuum window, Solar filters, calibration load, pass through hole on the cal. wheel) should be at least 4 beam radii at the lowest observing frequency (where the beam is larger) to incur in negligible truncation loss. For example, at 100 mm from the feed horn aperture the beam waist radius at 78 GHz is 24 mm and the minimum clearance aperture should be 96 mm (at that frequency).

The electromagnetic and mechanical designs of the INAF feed and OMT could be adopted for this project. The mechanical drawing of the assembly is shown in Fig. 18. The detailed mechanical drawings and the measurement results of the ALMA Band 2+3 prototype components will be provided (upon request, in the framework of a Non-Disclosure Agreement - NDA) to the company/consortium that will qualify to the final award phase of this OR1 tendering. However, INAF will not take any responsibility over the final performance results of such passive components. The awarded company can decide whether or not to adopt the INAF designs.

A re-imaging optics (for example based on a Gaussian Beam Telescope) could be adopted to reduce the angular spacing between the projected beams on the sky to a value of 2-2.5 HPBW at all frequencies without requiring miniaturization of the feed module and of the feed spacing on the focal plane. However, the re-imaging optics should induce negligible optical aberrations of the off-axis beams and the opto-mechanical mounting needs to fit within the allowed volume. In addition, it should add negligible noise (requiring low insertion loss), achieve high aperture efficiency, polarization efficiency, minimum truncation loss, minimum beam distortion and minimum beam squint.

If adopted, a re-imaging optics system for coupling the beams to the *shaped* SRT optics would need to be carefully designed.

5.4 W-BAND RECEIVER ARRAYS IN 4×4 AND 3×4 CONFIGURATIONS AND DESIGN OF MINIATURIZED CRYOGENIC MODULES

To fit a larger number of W-band pixels on the usable “high-efficiency” focal plane area of the shaped Gregorian SRT telescope (with no re-imaging optics), i.e. within a maximum diameter ≈ 130 mm, it is necessary to adopt smaller components and utilize non-standard W-band waveguide flanges. The representation of a possible 4×4 array

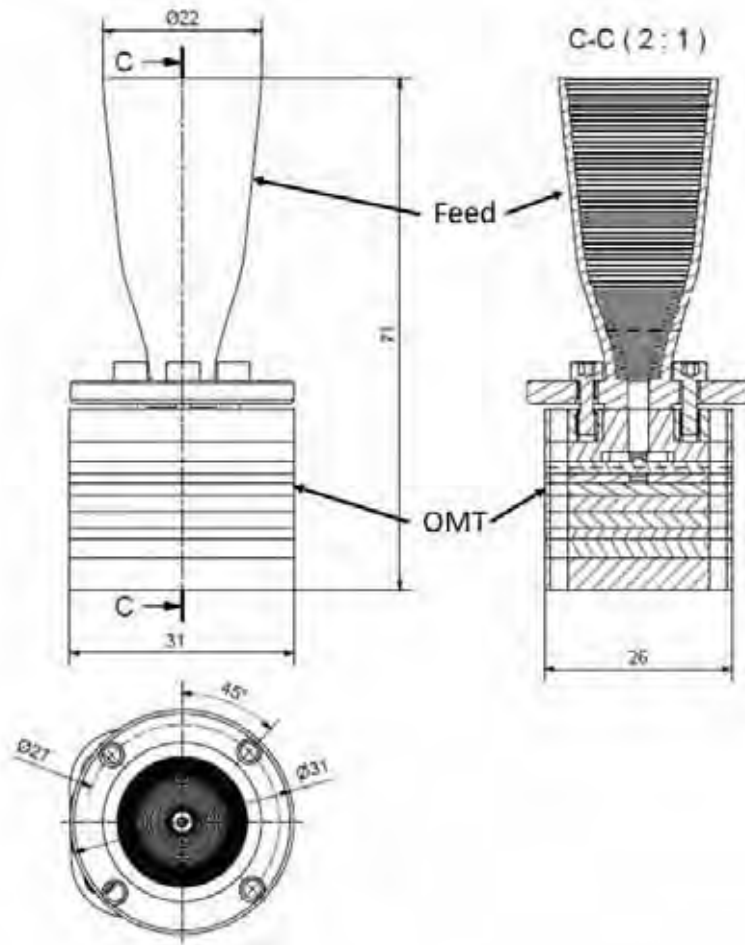


Fig. 18. Mechanical drawings of the platelet W-band feed-horn and OMT assembly with 31 mm footprint designed by INAF for the SRT Gregorian focus (70-116 GHz).

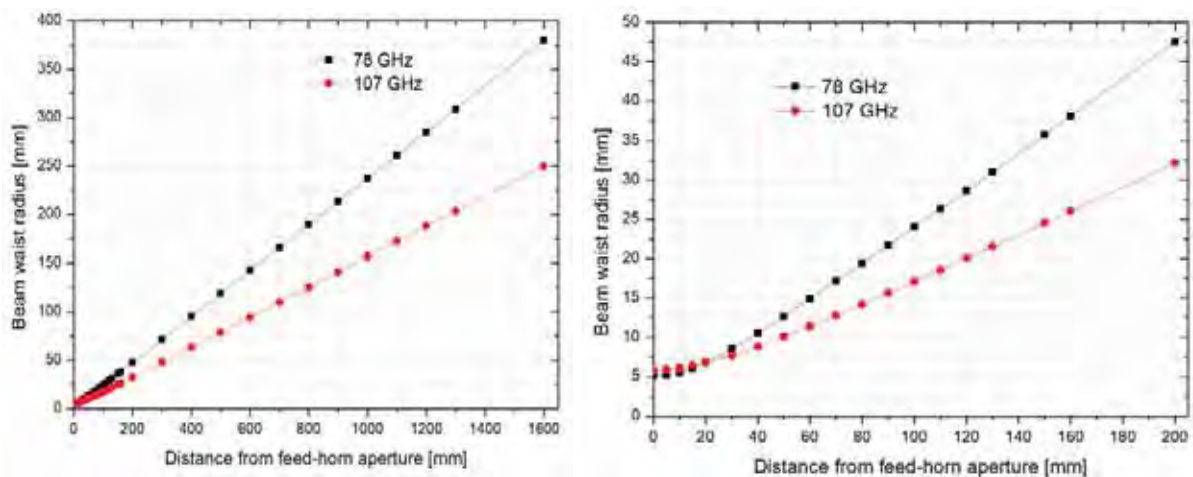


Fig. 19. Simulated beam waist radius (in mm) versus distance from feed-horn aperture (up to 1600 mm, left panel and up to 200 mm, right panel) of the feed-horn designed by INAF for optimum illumination of the SRT. The beam waist radius is provided at 78 GHz and 107 GHz.

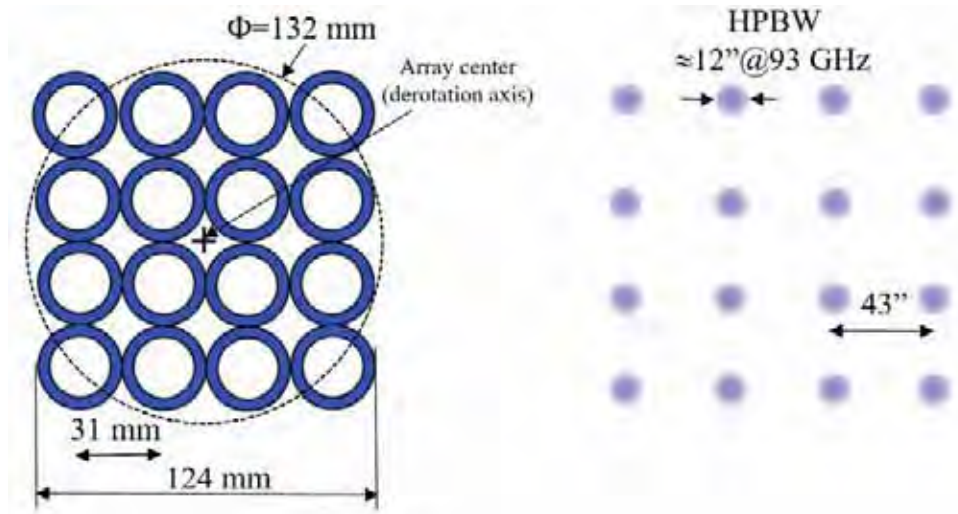


Fig. 20. Example of configuration of the array with 4x4 feeds on the Gregorian focal plane (left panel) and corresponding beams projected on the sky (right panel).

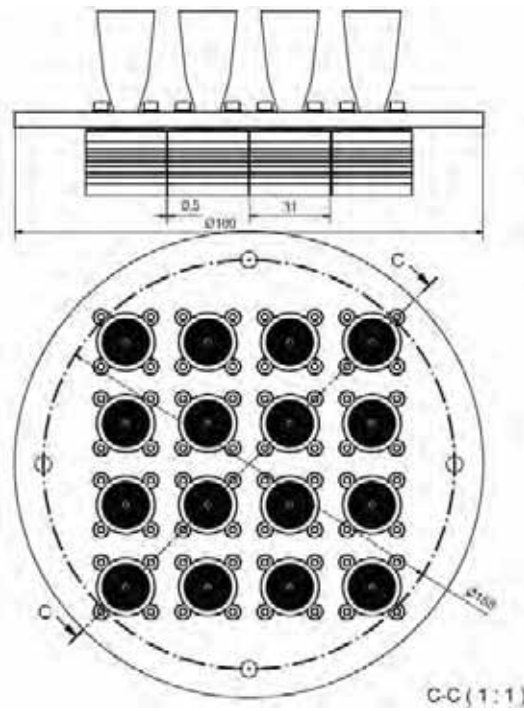


Fig. 21. Mechanical drawings of the W-band 4x4 array assembly of INAF feed-horns and OMTs.

configuration with ≈ 31 mm feed spacing and an illustration of the beam separation on the sky expected after coupling the radiated patterns of the feeds with the SRT optics are shown in Fig. 20. Adoption of a feed spacing of ≈ 31 mm requires to design the single-pixel modules (feed-horn, OMT and LNAs) with a maximum cross-section of $\approx 31 \times 31$ mm². Figure 21 shows a possible integration of the INAF feed-OMT assembly.

5.4.1 Cryogenic array based on dual-polarization LNAs

Figures 22 and 23 show a sketch of two possible W-band cryogenic arrays, respectively in 4×4 and 3×4 configurations, with ≈ 31 mm pixel spacing. Both architectures

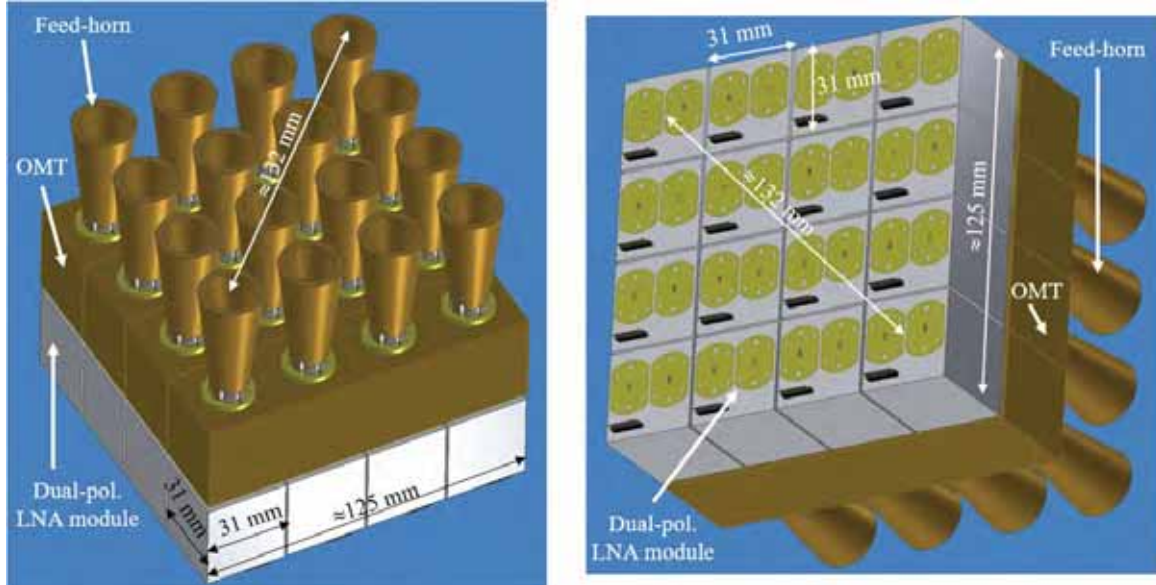


Fig. 22. Sketch of W-band 4×4 cryogenic array of pixels based on a cascade of a feed-horn with an OMT and with a dual-polarization LNA cryogenic module. The OMT waveguide outputs and the waveguides inputs and outputs of the dual-polarization LNA module utilize non-standard UG387 waveguide flanges (for example an UG387 flange with only two screws and with “cuts” that makes them fit into 15 mm spacing on the waveguide E-plane). View form the feed horns side (left panel) and from the dual-polarization LNA modules side (right panel).

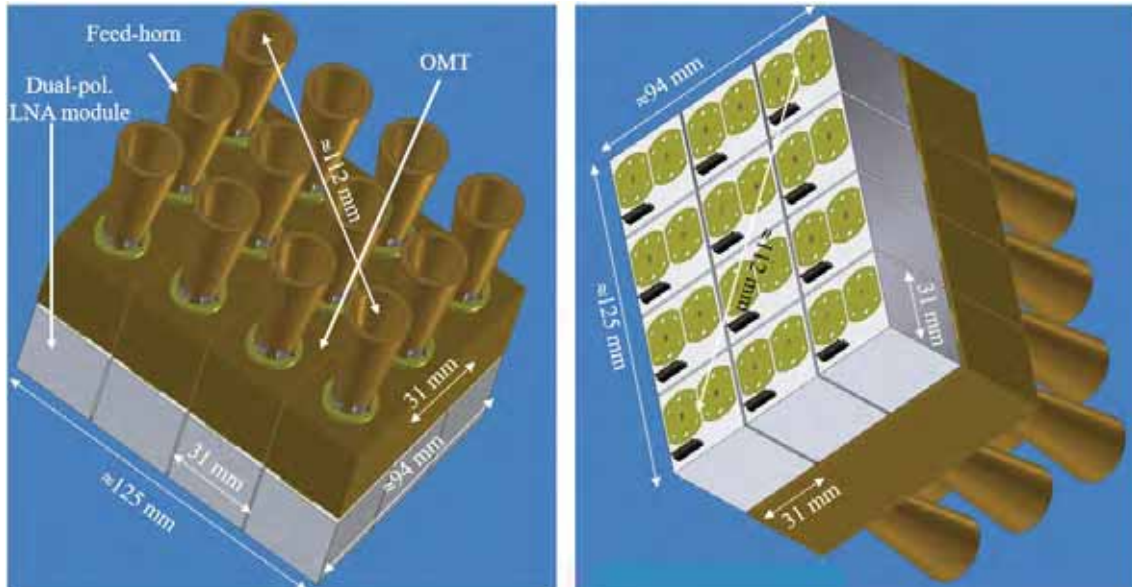


Fig. 23. Sketch of W-band 3×4 cryogenic array of pixels based on a cascade of a feed-horn with an OMT and with a dual-polarization LNA cryogenic module. The design of the elements is similar to that presented in Fig. 22.

are based on identical cascade of feed, OMT and dual-polarization LNA module. The dual-pol LNA would feature two waveguides at its inputs (and two waveguides at its outputs), one per polarization channel, and should deliver ultra-low noise performance across 70-116 GHz ($T_N \approx 25-40$ K) with approximately ≈ 45 dB gain and good matching at all ports.

5.4.2 Cryogenic array based on “active OMT”

An alternative design is based on an “active OMT” module. Such device consists of an OMT that integrates low noise amplification stages and could be similar to the one presented in [7]. 3D sketches of the W-band single-pixel module and of the 4×4 cryogenic array, based on an active OMT module are shown, respectively in Figs. 24 and 25.

5.5 CRYOGENIC LOW NOISE AMPLIFIERS

The specifications of the cryogenic LNAs depend on the adopted receiver architecture. They shall be chosen to guarantee a single side band receiver noise performance, when measured in front of the receiver vacuum window, of less than 70 K full-band for all

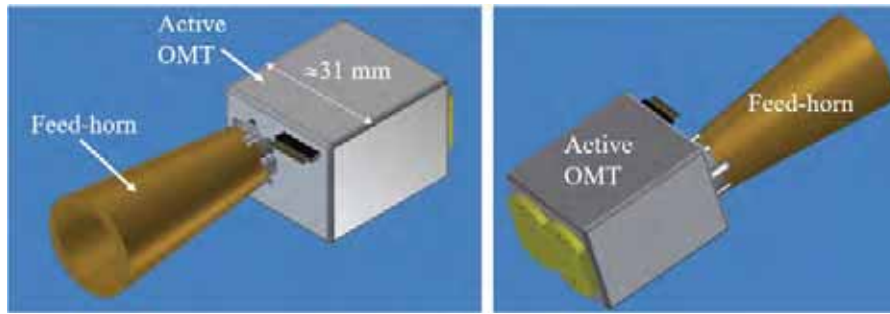


Fig. 24. Sketch of W-band single-pixel dual-polarization module based on “active OMT”. The DC connector could be placed on the input side (feed-horn side).

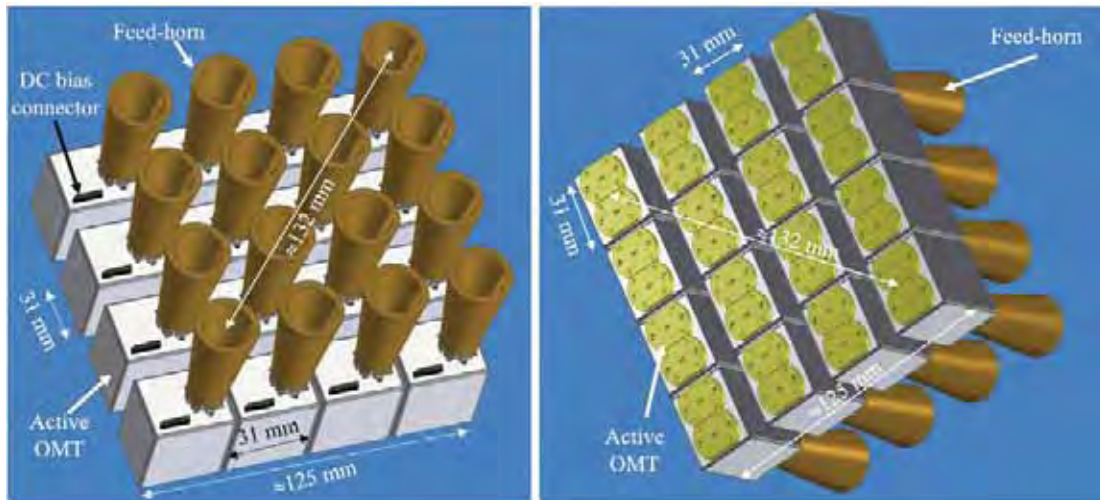


Fig. 25. Sketch of W-band 4×4 cryogenic array of pixels based on a cascade of a feed-horn with an “active OMT”, a dual polarization module based on low noise amplification stages. The active OMT waveguide outputs utilize non-standard UG387 waveguide flanges. View form the feed horns side (left panel) and from the active OMTs output side (right panel).



UNIONE EUROPEA
Fondo Sociale Europeo
Fondo Europeo di Sviluppo Regionale



pixels/polarizations across the 75-116 GHz band (goal 70-116 GHz). The receiver noise budget estimate (to be discussed in Sec. 6.4) indicates that the noise performance at the input of the first LNA stage should be $T_N < 35$ K. Here, we refer to the example of a receiver architecture consisting of two LNA modules in cascade for each of the polarization channels, as depicted in Figs. 5 and 13. The first cryogenic LNA module shall deliver ultra-low noise performance and a gain of order 23 dB. The total gain of the two LNA stages shall be carefully chosen to satisfy two opposed requirements: on one hand a high gain would be desired to reduce the noise of the following stages (down-converter, IF switch, fiber optics link, etc.) down to a negligible level; on the other hand, the receiver should have a linear response and operate well below the 1dB compression point. Therefore, the total gain of the 70-116 GHz cryogenic LNAs should be carefully chosen to avoid risk of saturation of the last LNA stage due to the large input bandwidths. The input power expected at the first cryogenic LNA input when observing a 300 K load is of order -65 dBm assuming an input bandwidth of ≈ 60 GHz. With a total gain of the two cascaded LNAs of ≈ 46 dB the output power of -19 dBm would run the last stage near the non-linearity regime if the LNA output $P_{1dB} \approx -10$ dBm. For solar observations, the equivalent Sun emissivity of ≈ 8000 K, would saturate the receiver.

Three solutions are proposed to mitigate this problem:

- a) drive the last LNA stage to higher current to get higher IP_{1dB} (≈ 0 dBm). This is possible if the amplifier gain does not increase with the driving current.
- b) use a single cryogenic LNA with gain of approximately 33 dB, enough to reduce the noise of the following receiver stages to a negligible level: the cryogenic LNA would be cascaded with a room temperature LNA with high P_{1dB} . It is unclear if a cryogenic LNA with ≈ 33 dB gain exists or could be produced, and if a room temperature LNA with high IP_{1dB} is available to cover the entire band of interest (70-116 GHz);
- c) reduce the RF input bandwidth injected into the LNAs chain using a band pass filter at the receiver input during solar observations (to be discussed further down).

The LNA module(s) should be designed to be compatible for integration with the other array elements (electrical/mechanical, DC connector and placement, number of biasing wires, etc.) and should comply with the cryogenic power requirements in terms of thermal power dissipation.

6 Receiver architecture, down-conversion schemes, power and noise budgets

As discussed in Section 3, the W-band multibeam receiver can adopt different architectures in terms of pixel number, down-conversion scheme and instantaneous band processed by the backend. See also Appendix D. From the point of view of the cryogenic array, three possible configurations with increasing number of pixels are summarized in Fig. 21: $3 \times 3 = 9$ pixels, $3 \times 4 = 12$ pixels and $4 \times 4 = 16$ pixels. The corresponding number of waveguide outputs of the dual polarization arrays are, respectively 18, 24 and 32. The cryogenic array is cascaded with conversion modules that can be located at room temperature or at cryogenic temperature. These modules convert the 3 mm-wave signals from one polarization channel of each pixel to one or two 1IF bands in the range 2-18 GHz

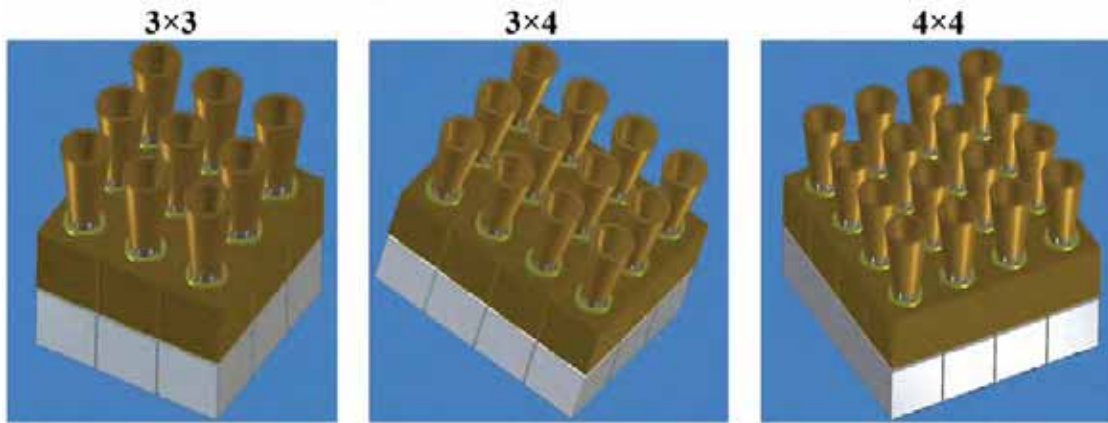


Fig. 26. Sketch of three possible configurations of the W-band cryogenic array based on a cascade of a feed-horn with an OMT and with a dual-polarization LNA cryogenic module: 3×3 array (left), 3×4 array (center), 4×4 array (right).

(or part of it, i.e. 4-12 GHz). Various down-conversion schemes can be adopted. For example, these can be based on sideband separation with sub-harmonically pumped mixers, delivering two 1IF bands per polarization channel or on single side band fundamental balanced mixers, delivering one 1IF band per polarization channel.

6.1 3×3 ARRAY WITH SIDEBAND SEPARATING DOWN-CONVERTERS

Here, we refer to Fig. 5, which shows a block diagram with a possible architecture of the W-band 3×3 receiver array and present its sub-systems and components with more details.

The architecture is similar to one adopted for the receiver developed in the framework of the Radionet Joint Research Activity AETHRA (Advanced European Technologies for Heterodyne Receivers for Astronomy) WP1 programme.

The design allows the three following types of observation: *a)* array of feed-horns pointed at the cold sky (weak radio astronomy signals); *b)* array of feed-horns pointed at the Sun (strong radio astronomy signal), after insertion of Solar filters in the signal path; *c)* array of feed-horns pointed towards a room temperature (296 K) calibration load, to be placed in front of the cryostat vacuum window.

The receiver employs three rows of three dual-linear polarization cryogenic chains located inside a cryostat and three modules of three-pixel down-converters based on sideband separating scheme located at room temperature, outside the cryostat.

The cryogenic section utilizes a cascade of feed, OMT and LNAs. We note that the feed and the OMT are directly connected to each other without polarizer (Differential Phase Shifter): the receiver will be sensitive to two orthogonal linear polarizations, not to two circular polarizations (full-Stokes capabilities are not a requirement).

The amplified signals available from the nine cryogenic dual-polarization feed-system are transported by $3 \times 3 \times 2 = 18$ waveguides to the receiver cryostat outputs grouped as three lines of six waveguides. We define with “H” and “V” the channels corresponding to the horizontal (Pol-H) and vertical polarization (Pol-V), respectively.



Waveguide band pass filters (BPF) are located at room temperature and are attached to the cryostat backplate in front of three down-converter modules. These are based on a sideband separating (2SB) mixer scheme utilizing GaAs semiconductor Schottky technology. The downconverter utilizes an RF hybrid, two sub-harmonic mixers (in second harmonic), and one IF hybrid. In the Schottky mixers, a strong LO sub-harmonic signal provided by an LO chain fed by an external phase-locked master synthesizer operating in the 14.5-17.4 GHz range is mixed with the 3 mm-wave astronomy signals received from the antenna at the USB and at the LSB. Thus, two 1IF outputs are available, one for each sideband.

Figure 27 shows a diagram of the frequency bands that can be covered with two different LO1 tunings, one for observing in the upper part of the 70-116 GHz frequency band (in red color, with $\nu_{LO1}=104$ GHz) the other for observing in the lower part of the 70-116 GHz band (in blue color, with $\nu_{LO1}=82$ GHz). The frequency ranges of the local oscillator at the LO1 frequency as well as the tripler output and at the first signal generator outputs are also shown in Fig. 27. We note that the entire 70-116 GHz band can be covered with four separate tunings of LO1. The unwanted LO harmonics should be filtered out or exhibit a negligible output power level to avoid the conversion of unwanted higher order RF sidebands.

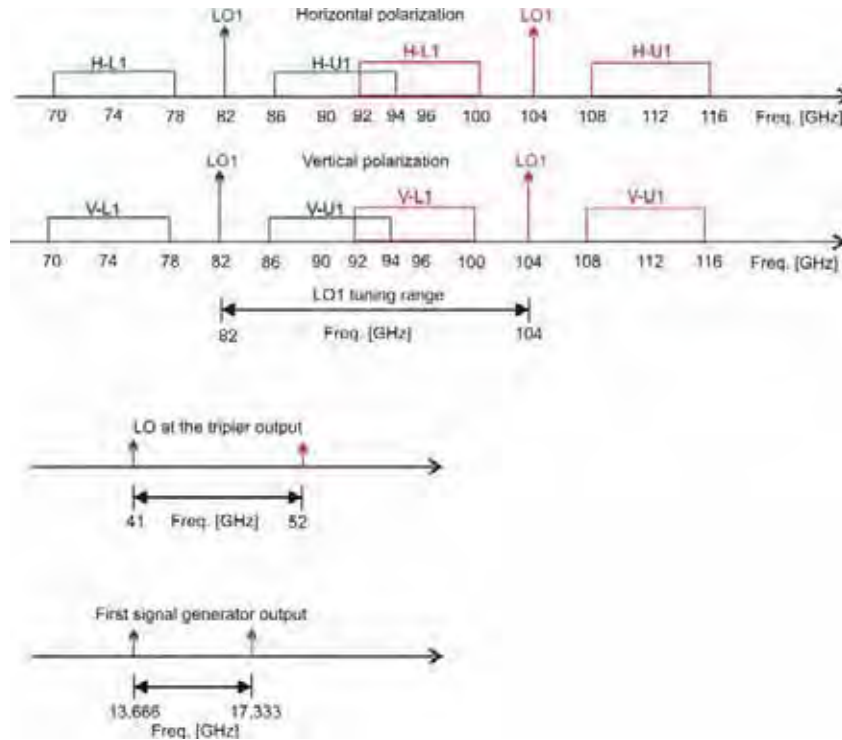


Fig. 27. Sideband separating down-conversion scheme (2SB) of the LSB (L1) and of the USB (U1) with 4-12 GHz 1IF (8 GHz bandwidth per sideband). Top diagram: down-converted bands with two different LO1 settings tuned for operations in the upper part of the 70-116 GHz band (LO1 at 104 GHz, red color) and in the lower part of the lower 70-116 GHz band (LO1 at 82 GHz, blue color). Both the Horizontal and Vertical polarizations are shown along with a diagram of the LO1 tuning range, 82-104 GHz. Bottom diagrams: local oscillator tuning ranges at the tripler output (41-52 GHz) and at the first signal generator output (13.666-17.333 GHz).



UNIONE EUROPEA
Fondo Sociale Europeo
Fondo Europeo di Sviluppo Regionale



The power level specification for the spurious harmonics of the LO will be determined according to the adopted down-conversion scheme (expected values of less than 30 dBc).

Each down-converter module receives the signals from a row of 1×3 dual polarization pixels, i.e. from 6 waveguides (for example 1H, 1V, 2H, 2V, 3H, 3V) and down-converts them to 12 × 4-12 GHz 1IF outputs. In total, the receiver delivers 36 outputs across the 4-12 GHz 1IF band, 18×USB and 18×LSB.

The mixers are pumped with a local oscillator signal provided by a commercial high-power signal generator (phased-locked with the 10 MHz antenna reference) delivering a tone tunable across the 13.666-17.333 GHz frequency range (14.5-17.333 GHz for 75-116 GHz baseline RF band). Such local oscillator signal is distributed to 6 × I/Q mixers located inside each down-conversion module, multiplied by a frequency tripler to the 41-52 GHz range (43.5-52 GHz), band pass filtered and amplified before its injection into the subharmonic mixer that doubles it to produce a final LO1 tone tunable in the 82-104 GHz band (87-104 GHz), as required for observations across the 70-116 GHz signal band (75-116 GHz).

The image sideband rejection of the first down-conversion depends on various parameters and should be greater than 10 dB at all frequencies across the 4-12 GHz 1IF band. Thus, two 8 GHz-wide sidebands centered at 8 GHz and separated by 2×8 GHz=16 GHz can be observed in one setting for each of the polarization channels.

The minimum bandwidth of each of the sidebands for each polarization channel of the downconverter shall be 6 GHz and must fall across the 4-12 GHz 1IF, for example across 4-10 GHz.

6.2 4×4 ARRAY WITH SINGLE SIDE BAND DOWN-CONVERTERS

Figure 28 shows a block diagram with a possible architecture of the scientifically preferred W-band 4×4-element receiver array, based on single side band SSB down-conversion scheme where each of the polarization channels of the 16-pixel array delivers one single 1IF output across 2-18 GHz (16 GHz instantaneous bandwidth per polarization channel) from the USB. The receiver utilizes a sideband separating scheme with LSB internally terminated (into a 50 Ω load). In total, the receiver delivers 32×[2-18 GHz] 1IF outputs and is based on fundamental mixers pumped by a sextupler (×6 frequency multiplier) local oscillator source cascaded with a booster amplifier and a bandpass filter to reject the unwanted LO harmonics. The LO harmonics that cannot be filtered out, which are present across the LO range, must exhibit negligible output power levels, estimated to be of less than 30 dBc. A W-band isolator (not shown) might be used in the down-conversion scheme for improved matching and isolation.

Figure 29 illustrates diagrams of the conversion scheme of the USB (LSB not shown) down to the 2-18 GHz 1IF band. The three diagrams show that the full 70-116 GHz frequency bands can be covered with three different LO1 tunings (LO1 frequency set at 68 GHz, 84 GHz and 98 GHz).

The minimum bandwidth for each pixel/polarization channel of the downconverter shall be 12 GHz and must fall across the 2-18 GHz 1IF, for example across 4-16 GHz.

Intermediate array architectures between the 3×3 2SB (presented in previous subsection) and the 4×4 SSB configurations are briefly described in Appendix D.

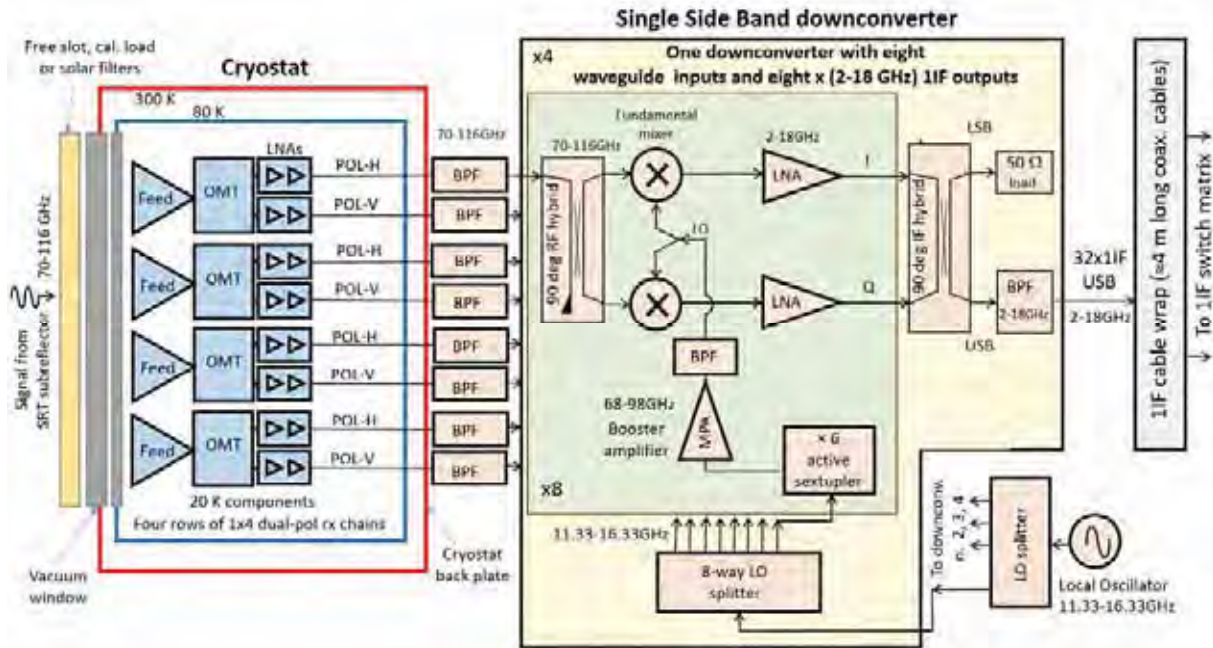


Fig. 28. Receiver architecture in 4x4 configuration showing the cryogenic components and the room temperature single side band USB down-converter delivering 32x1IF outputs across 2-18 GHz. The 32x1IF LSB outputs are internally terminated. The down-converter consists of four independent modules, each serving a line of four dual-polarization cryogenic pixels.

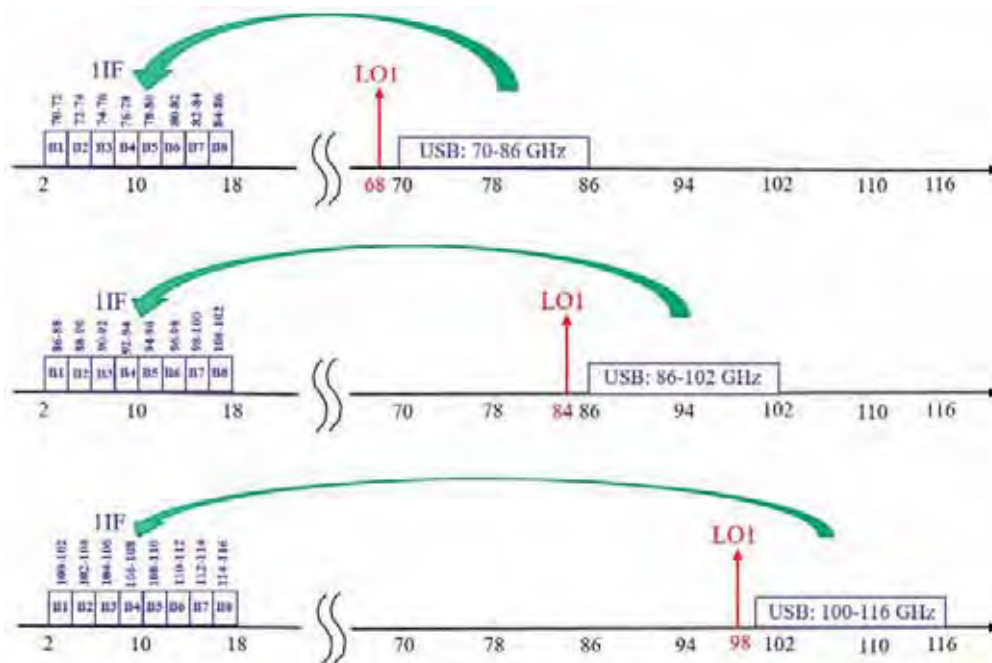


Fig. 29. Single Side Band (SSB) down-conversion scheme of the Upper Side Band (LSB rejected) with 2-18 GHz IF (16 GHz bandwidth). Only one of the polarization channels is shown. The diagrams refer to three different LO tunings: 68 GHz (top), 84 GHz (center), 98 GHz (bottom), down-converting the RF bands 70-86 GHz, 86-102 GHz and 100-116 GHz, respectively. The 2-18 GHz 1IF band is divided in 8x2 GHz-wide sub-bands, named B1-B8, also illustrated with the corresponding RF sub-bands.

6.3 1IF SIGNAL TRANSPORTATION AND INTEGRATION WITH OTHER RECEIVERS

Figure 30 shows a block diagram [8] of the overall signal and transportation and processing of the four future SRT receivers located at the Gregorian focus: W-band, Q-band, 3-band and K-band. The 1IF signals from these receivers are fed to the 1IF switch matrix that selects the 1IFs from the four different front-ends that will be available on the Gregorian receiver positioner. When the 1IFs from the W-band are selected, the signals delivered by the W-band receiver are transported through analogue fibre RFoF optics links (38×20 GHz links will be available⁴) to a second down-converter, named FBCB (Full Band Conversion/Continuum Board/Back-end), located outside the antenna in the data processing centre (CED). The FBCB, described in Appendix E, is cascaded with a digital backend (DBE) switch matrix that feeds the signals in parallel to different digital backends (DBBC, Abaco e Skarab). The 1IF switch matrix, the analogue fibre-optic links, the FBCB and the digital backends will be developed and provided by INAF: they will be shared with other Gregorian focus front-ends and are not considered to be part of the W-band receiver (they shall not be supplied).

The possible observing modes that will be possible to realize with the W-band receiver are described in Appendix E and detailed in [8].

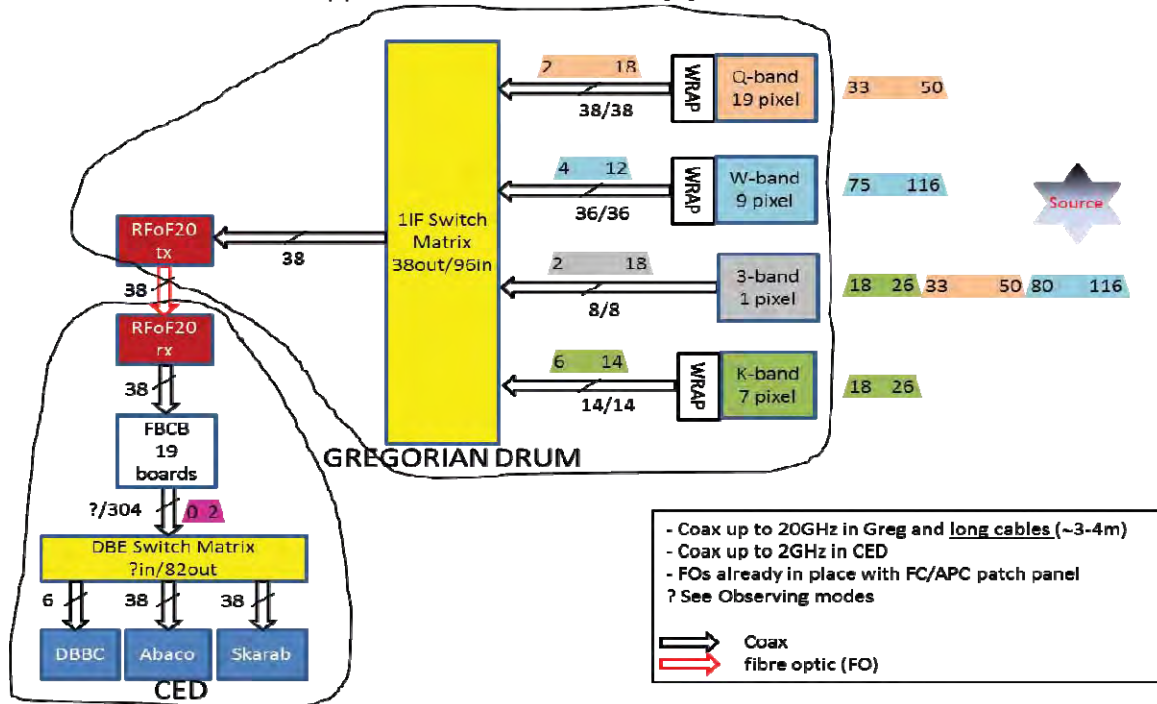


Fig. 30. Block diagram of the distribution of the IF signals from the receivers on SRT Gregorian focus down to the backend room (CED) using 20 GHz bandwidth analogue RF over Fiber (RFoF) fiber optics link, referred to as RFoF20. We assume the W-band receiver has 3×3 pixels with sideband separating configuration delivering 36×1 IF output signals 4-12 GHz to a 1IF switch matrix located in the Gregorian receiver positioner.

⁴ The maximum number of 1IF signals is set to 38 by the Q-band output signals (19 beams, dual polarization, 2-18 GHz 1IF band).

6.4 RECEIVER POWER BUDGET

For calibration purpose, the receiver array will observe a room temperature (≈ 300 K) load as depicted in Fig. 31. The calibration load will be switched in front of the receiver vacuum window. Here, we assume a sideband separating receiver architecture as in Fig. 5 and provide preliminary rough estimates of the noise budgets through the chain when the instrument observes: *a)* the room temperature calibration load; *b)* the cold sky; *c)* the Sun through solar filters. The integrated powers across the 1IF band at the 4-12 GHz outputs of the 1IF cable wrap are, respectively ≈ -30 dBm, ≈ -35 dBm and ≈ -26 dBm. If a different receiver scheme is adopted (for example an SSB architecture with 2-18 GHz 1IF outputs) the values will be 3 dB greater (doubling the 1IF band). In both cases, the power values at the 1IF outputs are in the linearity range of the following RFoF fiber-optic links. The receiver chain should be dimensioned to target for the above 1IF power level values at the cable wrap outputs. If required, additional 1IF amplifiers or attenuators (fixed or remotely controlled) shall be included in the receiver design (presumably in cascade to the 1IF BPF).

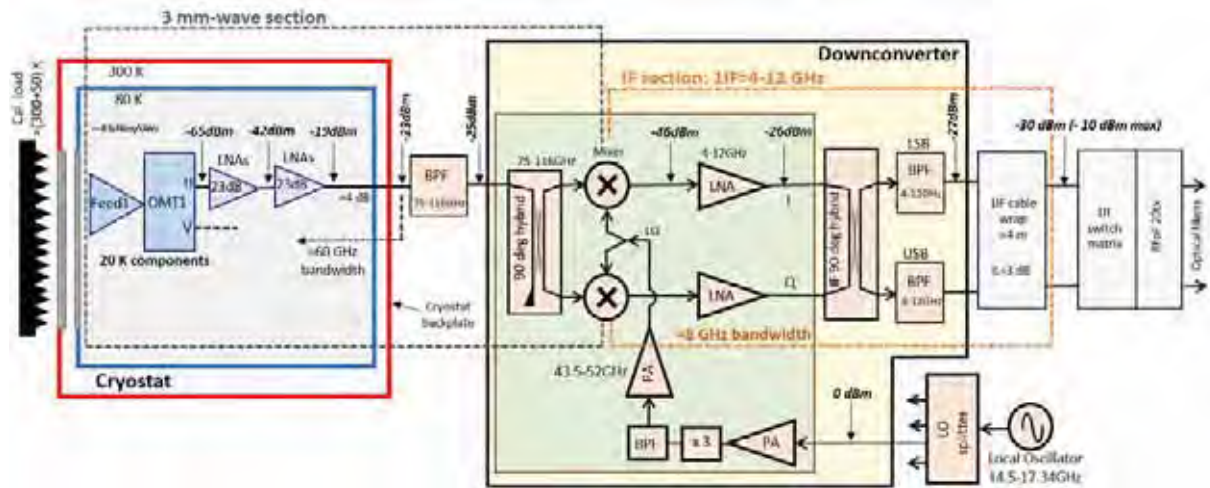


Fig. 31. RF power budget of the W-band receiver with architecture as of Fig. 5.

6.4.1 Power budget with receiver looking at a room temperature load

If the receiver noise referred to the vacuum window input is of order ≈ 50 K, a system noise power density of ≈ 350 K will be injected into the first stage LNA, equivalent to ≈ -83 dBm/GHz. If the input noise bandwidth is ≈ 60 GHz (≈ 60 -120 GHz) the integrated power at the input of the first LNA will be ≈ -65 dBm. Following two stages of amplification (≈ 46 dB gain) and losses due to signal transportation, the integrated power available at the cryostat backplate output will be of order -23 dBm. Supposing that the down-converter (cascade of sideband separating mixer and IF LNA) delivers no gain and that the insertion loss of the 1IF cable wrap with 4 m long cables is ≈ 3 dB, the integrated power available at the 1IF switch matrix and RFoF fiber optics link will be of order -30 dBm. In the calculation, we accounted for the reduction of the band from ≈ 60 GHz to ≈ 8 GHz.

6.4.2 Power budget with receiver looking at the cold sky

If the receiver is coupled to the SRT optics and observes the cold sky, rather than the 296 K calibrator, the system noise power density injected into the first stage LNA will depend on the atmospheric transparency, antenna elevation angle, spillover, etc. Its value is expected to vary in the range ≈ 100 -200 K during observation (expected to be ≈ 150 K during average weather conditions). See Appendix C. With a minimum system noise at the receiver input of ≈ 100 K the integrated power at the output of the 1IF cable wrap would be of order -35 dBm.

6.4.3 Power budget with receiver looking at the Sun through solar filters

The Sun emissivity across W-band is expected to be equivalent to a ≈ 8000 K load. To avoid saturation of the second cryogenic LNA stage the total RF power incoming into the receiver could be reduced by ≈ 10 dB (to ≈ -38 dBm) by RF solar filters (centered at 78 GHz and 110 GHz) with $\approx 6\%$ relative bandwidth (bandwidth reduction from ≈ 60 GHz to ≈ 6 GHz). The integrated total power at the input of the first cryogenic LNA would be of order -61 dBm and the integrated power at the output of the 1IF cable wrap would be of order -26 dBm.

6.5 RECEIVER NOISE BUDGET

Noise budget breakdown considerations are provided here to help the supplier to determine the sub-system specification. The Friis's formula was used to estimate the receiver noise referred to its input, which depends on the noise and gain of a cascade of stages. We assumed that the two cryogenic LNAs have the same gain (23 dB) and noise temperatures 30 K and 50 K, respectively for the first and second stage modules. The noise contribution added by the passive components (vacuum window, IR filter, feed-horn, OMT, waveguide sections, BPF, coaxial cables, etc.) depends on their insertion loss and on their physical temperature. For the W-band cryogenic receiver the noise of the input section in front of the LNA is the aggregate of the thermal radiation arising from small losses at various temperatures ranging from room temperature (≈ 300 K) down to the cryogenic operating temperature (≈ 15 -20 K). The losses incurred at room temperature, due to the vacuum window, are the most harmful to the noise and should be minimized.

Figure 32 shows a schematic of the full receiver chain with indication of the expected noise referred to its input, $T_{rec} \approx 47$ K. The values of the physical temperature, the power loss and the noise contribution are indicated in Fig. 32 for each of the stages. These values are also listed in Table 2.

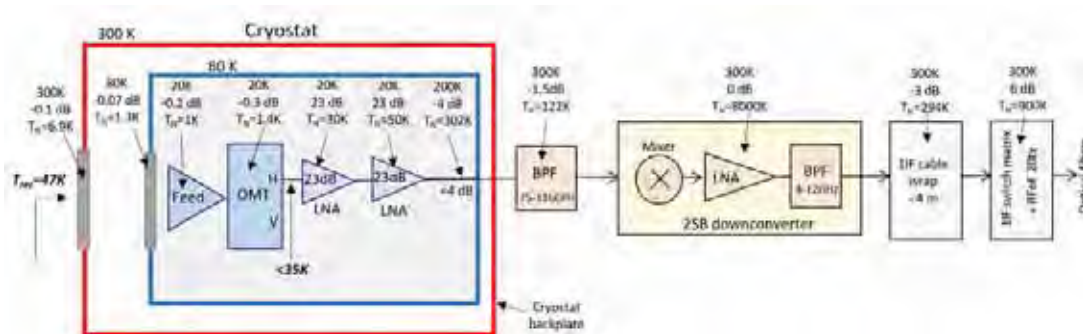


Fig. 32. Schematic of W-band receiver with noise budget estimates (receiver architecture of Fig. 5).



Component	Noise [K]	Physical temp. [K]	Gain [dB]	Noise contrib. [K]
Vacuum window	6.9	300	-0.1	6.9
Infrared filter	1.3	80	-0.07	1.3
Feed-horn	1	20	-0.2	1
OMT	1.4	20	-0.3	1.6
LNA first stage	30	20	23	35
LNA second stage	50	20	23	0.3
Signal wg transport	302	200	-4	0.01
75-116 BPF	122	300	-1.5	0.01
Down-converter	8000	300	0	0.8
IF cable wrap	294	300	-3	0.03
Total			≈ 37	≈ 47

Table 2. Receiver noise budget estimates (referred to Fig. 32).

6.6 RECEIVER CALIBRATION

The baseline calibration method for the receiver utilizes a single room temperature calibration load, an absorbing material at 296 K (for example Eccosorb from Emerson&Cuming Inc.) to be placed in front of the vacuum window, as depicted in Fig. 5. Such material absorbs the RF power and minimizes reflections, thus reproducing a “blackbody” that provides a temperature reference scale for all dual-polarization feeds of the array.

A more complex calibration scheme utilizes two absorbing loads, one at room temperature, the other at the cryogenic temperature of ≈ 77 K or ≈ 20 K. The blackbody emission of the cryogenic load could be coupled into the array feeds through suitably designed optical systems. The cryogenic load could be located inside an external cryostat or inside the W-band receiver cryostat, as long as they fit in the available space on the GRD.

Alternative calibration schemes could be proposed, which would need to be discussed during the competitive dialogue. One of these utilizes an amplified noise diode source coupled to an antenna that illuminates simultaneously all feeds of the W-band array from the SRT sub-reflector.

The INAF receivers currently installed on the SRT (L-P band, high-C band, K-band) use a noise source and a device to couple a specific amount of attenuated Excess Noise Ratio (ENR) into the receiver chain. The SRT does not have a fast nutating secondary or wobbler to remove the instrumental and atmospheric effects during observations. Ideally, the W-band multibeam receiver would include, for each of the pixels, a fast-switchable noise calibration system (min 100 Hz) to track the drift of receiver gain up to the knee frequency of the LNAs. The noise sources would be calibrated in the laboratory, before shipping the receiver to SRT, for example by measures with calibration loads at the temperature of the liquid Nitrogen (77 K) and at room temperature (296 K). The noise calibration coupling should be chosen to provide a noise calibration value around 10% T_{sys} and negligible when the calibration diode is switched off (average $T_{\text{sys}} \approx 150$ K).

7 Overall mechanicals, electrical and additional requirements

We present the preliminary design of a possible overall mechanical structure of a W-band receiver with architectures described in the previous section and show the mechanical interfaces between some of its sub-systems.

7.1 MECHANICAL ARRANGEMENT

Figure 33 shows the proposed mechanical layout of the receiver and of its main sub-systems. The main parts of the instrument are the following: 1) cryogenic focal plane array with feeds, OMTs and LNAs; 2) cryostat with CTI cryogenerator and vacuum components (including vacuum window and IR filter); 3) downconverter(s); 4) solar filters and calibration load switching system in front of the receiver vacuum window; 5) cabinet with electronics racks; 6) mechanical derotator and cable wrap with 11F coaxial cables and helium lines; 7) mechanical support frame for bolting to the Gregorian receiver positioner.

The main mechanical dimensions of the receiver are shown in Fig. 34. We note that the feed-horn phase centre must be positioned with precision with respect to a point located on the mechanical support frame: the feed phase centre shall be 21 mm above the mechanical reference “A”, visible on the right panel of Fig. 34. In the case of the feed

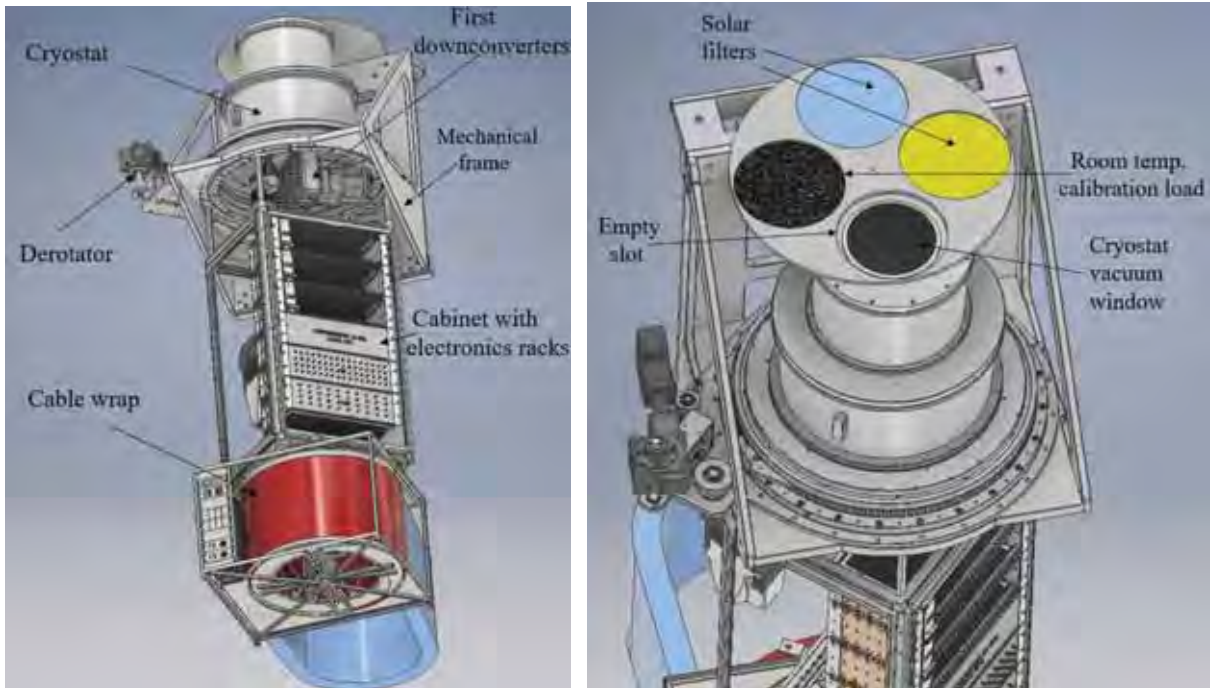


Fig. 33. 3D sketch of the W-band multibeam receiver for the Gregorian focus of SRT. View of the full instrument showing the cryostat with down-converter, mechanical derotator, cabinet with electronics rack and mechanical frame for mounting on the Gregorian receiver positioner (left). Rotating wheel for selection of Solar filters, calibration load or empty slot (right panel). The view shows the selection of the empty slot with the receiver looking at the cold sky.



UNIONE EUROPEA
Fondo Sociale Europeo
Fondo Europeo di Sviluppo Regionale

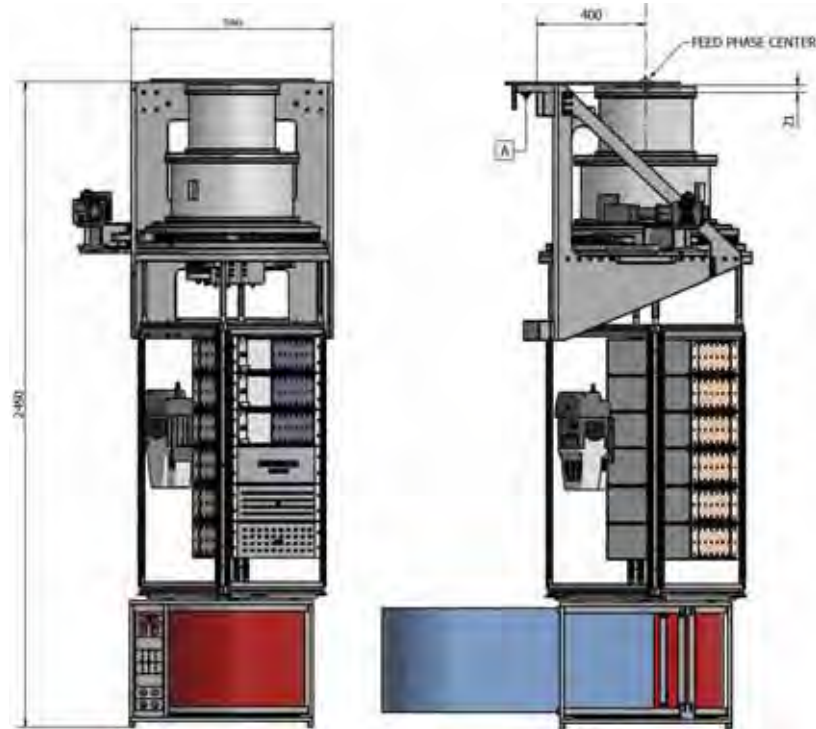


Fig. 34. Side views of W-band receiver with mechanical dimensions (in mm) and indication of the feeds phase center with respect to the mechanical reference (A) on the Gregorian turret (right figure).

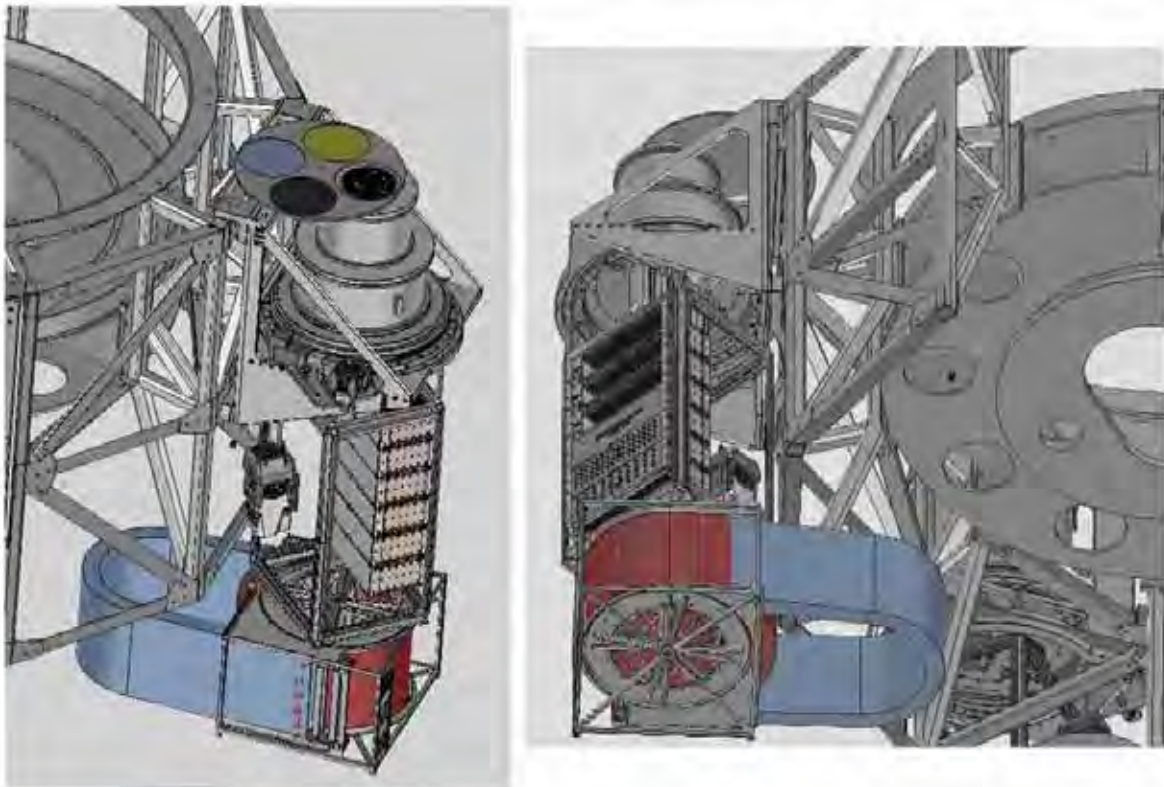


Fig. 35. 3D sketch of the W-band multibeam receiver mounted on the Gregorian rotating turret.

designed by INAF the phase centre is close to the feed aperture at all frequencies across 70-116 GHz. The array centre, shown in Fig. 14 for the 3×3 array and in Fig. 20 for the 4×4 array, shall coincide with the rotation axis of the mechanical derotator and be centred with respect to the mechanical support frame.

Figure 35 shows images of the receiver mounted on the Gregorian turret.

7.2 CRYOSTAT WITH CTI CRYOGENERATOR AND VACUUM COMPONENTS

In this sub-section we describe the important cryostat components, including the cryogenerator, the vacuum window and IR filter, the vacuum system and the monitor&control modules.

7.2.1 CRYOGENERATOR AND HELIUM GAS LINES

The design of the cryogenic components and of the cryostat assembly (choice of LNAs, number of LNA bias wires, infrared filter, etc.) shall minimize the thermal power dissipation to allow proper cooling of the parts by a single close-cycle helium refrigeration commercial cryogenerator (cryocooler). The cryocooler, based on the Gifford-McMahon thermodynamic cycle, must be compatible with the compressor (model CTI 9600) and helium lines that will be available at the SRT and shall be either a Cryodyne model CTI 350CP⁵ or model CTI 1020 from Helix Technology Corporation, now part of Brooks Automation Inc.. Both models adopt two cryogenic stages. Model CTI 350CP provides a heat lift of 4 W at 20 K and 20 W at 77 K simultaneously, while model CTI 1020, designed for higher capacity application, provides 12 W of heat lift at 20 K and 35 W at 77 K simultaneously.

The CTI 9600 compressor can drive one CTI 1020 or three CTI 350CP. Thus, the lower capacity CTI 350CP model must be preferred, if cryogenic thermal power considerations allow that choice. The CTI 9600 compressor is located in the antenna Alidade Equipment Room (see Fig. 1). The cryocooler, bolted to the receiver Dewar on the Gregorian Receiver Positioner, is connected to the compressor with ≈90 m long helium gas supply and return line. If the CTI 350CP cryocooler is adopted one single helium gas supply and return line can be shared by different receivers. Currently, all the receivers designed by INAF installed on the SRT, including the K-band multibeam receiver, adopt the CTI 350CP cryocooler.

The W-band receiver must be supplied fully equipped with CTI cryocooler and ≈4 m long 0.5" diameter self-sealing flexible interconnecting helium gas lines, to be located in the cable wrap along with the 11F coaxial cables.

The compressor is not part of the deliverables (already available at SRT), although it is required for testing purposes of the W-band receiver before this is delivered to the SRT. The array components at cryogenic temperature must be in thermal contact with the ≈15-20 K cold finger of the CTI cryocooler and must operate at a physical temperature of ≈20 K to deliver the required performances for all pixel elements.

⁵ <https://www.brooks.com/support/technical-support/documentation/cryochillers-cryocoolers/~media/Files/Support/Documentation/Vacuum/WaterpumpChillers/Manual%20Cryocoolers/8040272.pdf>

7.2.2 Vacuum window and Infrared filter

The material, diameter and thickness of the cryostat vacuum window shall be chosen to support the atmospheric pressure (with sufficiently high security factor) and reduce its bending to a negligible level in order to avoid phase distortions of the propagated beams. The window diameter must guarantee negligible truncation loss for all receiver beams and be dimensioned to provide 4 beam waist radii at the lowest observing frequency (see Sec. 5.3 and Fig. 19). The array must be confined within a ≈ 130 mm diameter. If located close to the feed apertures, where the beams are narrow, the vacuum window could have a 200 mm clear aperture (see Fig. 36) and consist of HDPE (High-Density Polyethylene) with ≈ 12 mm thickness (corrugations excluded). The Infrared Filter (IR) could consist of PTFE (Poly Tetra Fluor Ethylene) with 200 mm clear aperture and ≈ 6 mm thickness (corrugation excluded).

The refractive index $n=(\epsilon_R)^{0.5}$ and loss tangent $\tan \delta$ for HDPE are respectively, $n=1.53$ and $\tan \delta=3 \times 10^{-4}$ at $\nu \approx 100$ GHz at ambient temperature. The absorption loss per unit length α for HDPE is ≈ 0.06 dB/cm. In general, the loss per unit length is proportional to frequency ν and given by $\alpha=(2 \pi \nu n \tan \delta)/c$. Therefore, the thickness of the vacuum window shall be

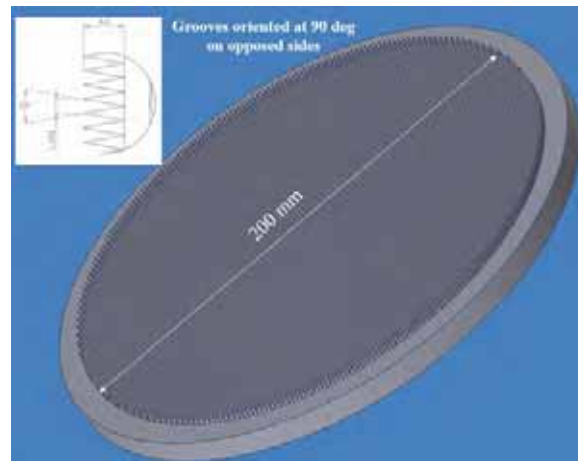


Fig. 36. Sketch of wideband vacuum window or IR filters with ≈ 200 mm clear aperture. The corrugations have triangular shape with 20 deg angle and 4.8 mm depth (designed at IRAM for ALMA Band 2+3 and adopted for the NOEMA Band 1 receiver).

minimized to reduce its insertion loss, as this increases linearly with thickness and strongly impact the receiver noise temperature because is located at room temperature (as discussed in Sec. 6.5).

Triangular corrugations machined on each side of the windows/filters would provide wideband anti-reflection coatings (Fig. 36).

7.2.3 Cryostat and vacuum system

The main parts of the cryostat are the vacuum window and Infrared Filters, the vacuum enclosure, the ≈ 80 K screens plus thermal links to connect the internal ≈ 15 -20 K stage, the waveguide and DC vacuum feedthrough for connecting the RF signals and bias



UNIONE EUROPEA
Fondo Sociale Europeo
Fondo Europeo di Sviluppo Regionale



Fig. 37. 3D sketch of the inner part of the cryostat showing the 4×4 cryogenic array and the CTI cryogenerator (cold finger). Left panel: the vacuum window is located in front of the feed-horn cluster. Right panel: view of the 4×4 array.

wires for the LNAs and readings of the cryogenic temperature stages. On its front-plate, the cryostat should incorporate the vacuum window and the IR filter as depicted in Figs. 37-38.

On its backplate, the cryostat shall incorporate the CTI cryocooler (model 1020 or 350CP), the pressure gauge, the electromagnetic valve, the bias connectors (for the active parts of the cryogenic array and for monitoring the cryogenic temperatures) and the mechanical flange(s) with vacuum waveguide feedthroughs. An example of the cryostat backplate based on a single mechanical flange with waveguide vacuum feedthroughs are depicted respectively in Figs. 38 and 39. This mechanical flange is the interface between the cryostat and the room temperature parts of the receiver, where the band pass filters (BPFs) and the following downconverter module(s) will be connected. Views of the backplate from the “external” side (downconverter side) and from the “internal” cryogenic/vacuum side are shown, respectively on the left panel and on the right panel of Fig. 38.

Various design options are possible for the cryostat backplate and for the mechanical vacuum waveguide feedthroughs, which could be grouped, miniaturized, based on non-standard waveguide flanges, and mounted on single or multiple mechanical vacuum flanges.

Vacuum sealing through the waveguide signal path should consist of a low-loss, low-input reflection broadband waveguide vacuum window with low leak rate ($< 10^{-8}$ mbar l/sec). This could be based on a thin Mylar sheet ($\approx 25 \mu\text{m}$) clamped between waveguide flanges with an O-ring seal, or on alternative broader band hermetic designs with low leak rates.

The cryostat design will include thermal breaks and superinsulation layers to minimize the thermal power into the cryogenic stages and guarantee an appropriate cooling of the array. In particular, the signals at the outputs of the cryogenic low noise amplification stages shall be transported to the cryostat backplate using low thermal conductivity transmission lines, based for example on Gold-plated stainless-steel waveguides, broadband thermal isolators by waveguides gap, or dielectric waveguides. The cryostat could consist of two coaxial cylindrical sections (see Fig. 33-36) in order to minimize the Infrared radiated load on

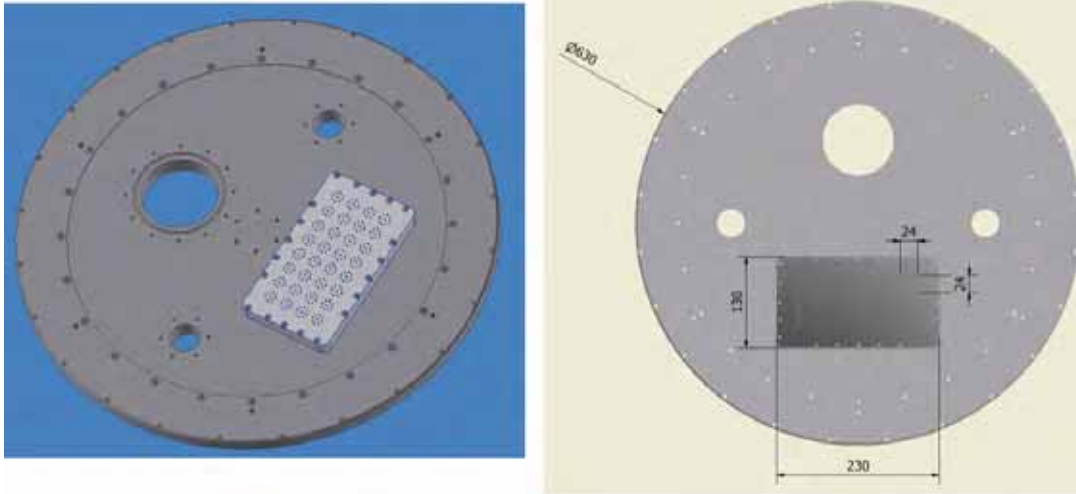


Fig. 38. 3D sketch of the cryostat backplate mounted with 32 vacuum waveguide feedthroughs on a mechanical flange (4x4 array configuration).

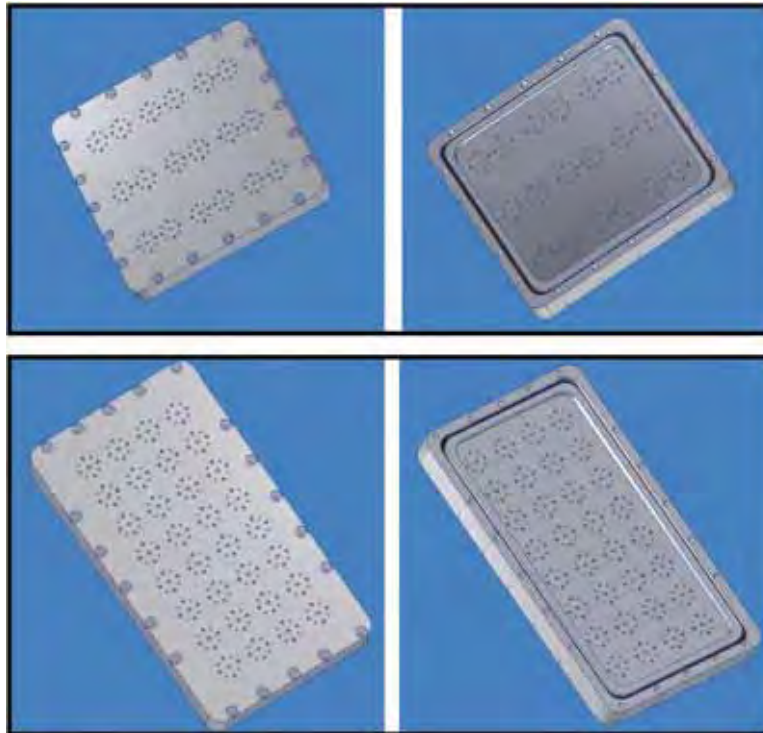


Fig. 39. Examples of single mechanical flange with 18 vacuum waveguide feedthroughs for 3x3 array (top panels) and with 32 vacuum waveguide feedthroughs for 4x4 array (bottom panels). The images on the right panels show the channel for the vacuum-seal O-rings surrounding the waveguide feedthroughs.

the coldest stage: the cryogenic array (≈ 130 mm diameter) and the supports for the vacuum window with Infrared Filters could be confined in a cryostat section with diameter ≈ 300 mm, while the CTI cryogenerator, vacuum gauge and electromagnetic valve, could be hosted on a larger cryostat section with diameter ≈ 630 mm (see backplate drawings in Fig. 38).



UNIONE EUROPEA
Fondo Sociale Europeo
Fondo Europeo di Sviluppo Regionale



The supplier shall carry out a thermal study of the fully equipped cryostat and provide reports on design, vacuum tests and cryogenic tests.

The outer part of the larger cryostat section should be designed to incorporate a mechanical interface for connection to the mechanical derotator, whose drawings will be provided by INAF: the Dewar (with focal plane array inside it) and the cabinet with electronics rack (Fig. 33 left panel) will be rotated by the mechanical derotator during the observation.

Vacuum pumps (Agilent IDP3A01 primary pump and Agilent MDP5011 turbo drag secondary pump) and a vacuum gauge (WRG-D-NW25) shall be permanently installed and connected to the receiver cryostat while in operation on the SRT telescope. An electromagnetic vacuum valve (Edwards IPV16EKA) must be installed between the Dewar and the turbo molecular pump to guarantee the necessary low vacuum pressure in the Dewar chamber while the turbo molecular pump is off and the vacuum valve is closed. The turbo molecular pump is controlled by the Adixen ACT 200 TH. A switch relays box is required for switching on and off the primary pump, the CTI cold head and the vacuum valve. Fig. 40 shows photos of the main parts of the vacuum system.

7.2.4 Monitor and control module

The vacuum valve, the turbo molecular pump, the primary pump and the CTI cryocooler must be remotely controlled and monitored. For maintenance purposes, the cryostat vacuum pressure shall be permanently and remotely monitored by the vacuum gauge. Fig. 41 shows the proposed rack with modules for monitoring and control of the cryogenic stages. These modules are compatible with the existing SRT antenna control software.

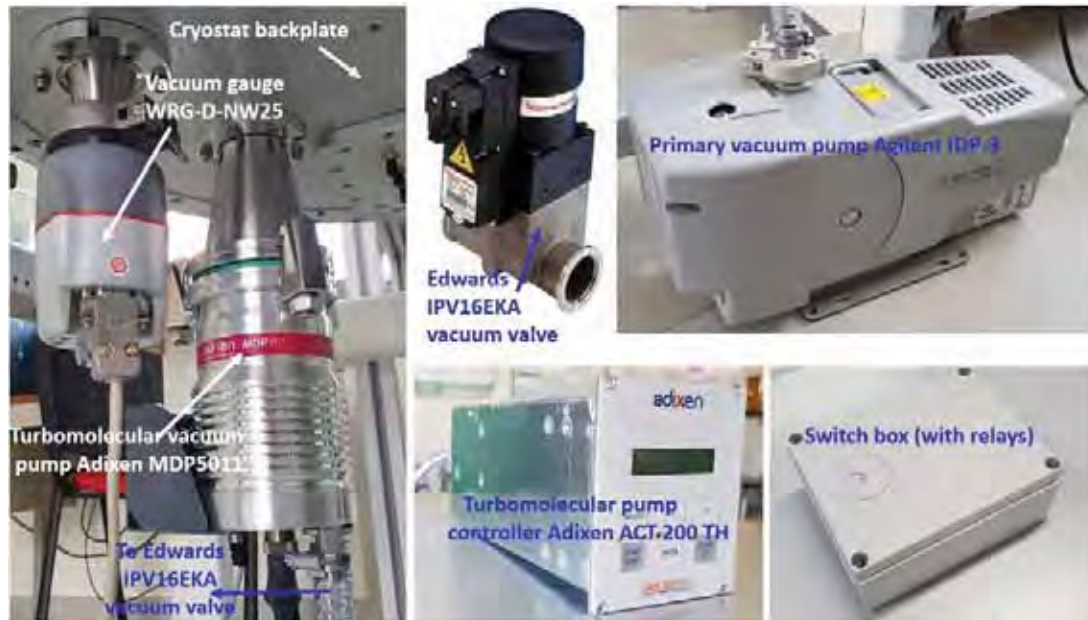


Fig. 40. Photos of vacuum system parts to adopt for the W-band receiver. The image on the left panel shows the vacuum pump and vacuum gauge attached to a laboratory cryostat. The vacuum valve shall be cascaded to the vacuum pump.

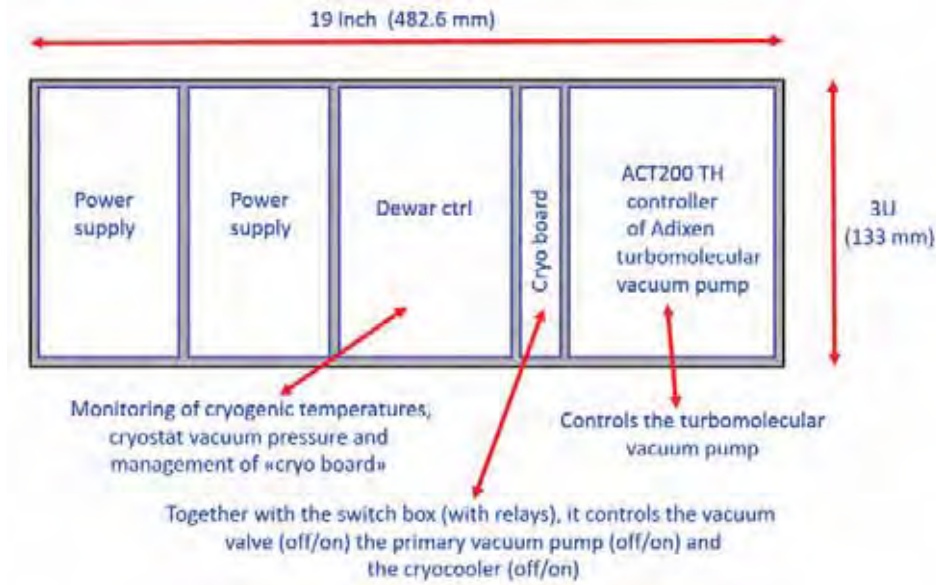


Fig. 41. Example of the electronics rack for monitoring and control of the cryogenic system.

Description	Brand	Model	Code
Dry Scroll primary vacuum pump	Agilent Technologies	IDP3A01	
Turbo drag high-vacuum secondary pump	Pfeiffer Vacuum	MDP5011	795601
Turbo pump controller	Pfeiffer Vacuum	ACT 200 TH	20004
Electromagnetic vacuum valve	Edwards	IPV16EKA 240V	C41610000
Vacuum Gauge	Edwards	WRG-D-NW25	D14702000
Cryocooler	CTI Cryogenic	CP350 or CP1020	
Cryogenic temperature sensors	Lake Shore Cryotronics	DT-670B-CU	

Table 3. List of the main vacuum and cryogenic system parts that must be adopted (and supplied) for the W-band receiver.

The receiver shall include a monitoring of the temperatures of the two cryostat cryogenic stages (≈ 15 -20 K and ≈ 80 K) with at least four Silicon diode temperature sensors (Lake Shore Cryotronics model DT-670B-CU): two sensors placed in thermal contact with the cold fingers at ≈ 15 -20 K and ≈ 80 K (one for each stage), one sensor placed on one of the LNAs of the cryogenic array (at ≈ 15 -20 K) and one placed on the IR shielding at ≈ 80 K.

A list of the vacuum system components that must be adopted for the W-band receiver is provided in Table 3. The vacuum system must include all accessories for its full on-site operation (Air Cooling kit for MDP5011, all cables, vacuum adapters, O-ring vacuum sealing, etc.).

7.3 LNA BIAS AND MONITOR&CONTROL

The cryogenic LNAs of the W-band receiver must be biased and monitored using bias modules developed by INAF. Two versions of the LNA board have been developed. Both

printed circuit board versions are rack-mountable and based on standard Eurocard 3U format with 5 horizontal pitch width (5 HP=25.4 mm) and 160 mm depth. The choice of the adopted LNA board solution will be discussed and agreed during the competitive dialogue. INAF will provide the necessary information to the awarded supplier for the acquisition of the chosen LNA boards.

7.3.1 Analogue LNA bias board

Fig. 42 shows a photo of the LNA bias boards adopted for the 14 LNAs of the K-band multibeam receiver (named ALISRT). Seven bias boards are used (Feed 0 to Feed 6) to bias the 7 dual-polarization feed system. Each rack-mountable board is based on analogue potentiometers for setting the drain voltage V_d and the drain current I_d for 10 amplification stages (five for polarization channel). Another dedicated board, based on a microcontroller and Analogue to Digital Converters, can remotely monitor the V_d , I_d , V_g for each of the 10 channels. In total, the seven boards, can monitor up to 70 LNAs.



Fig. 42. Photo of the ALISRT+dewar control of the K-band multibeam receiver based on seven analogue bias monitor LNA boards.

7.3.2 New digital LNA bias board

Fig. 43 shows the new four-layer programmable digital LNA bias board (named GAIA) recently developed at INAF. Each board is based on a microcontroller and on digital potentiometers for remote setting and control of the drain and gate voltages, respectively V_d and V_g , for 10 amplification stages (five for polarization channel). The procedure for setting up the bias voltages to its goal values, when switching on the LNAs, is reached incrementally from the 0 V condition and is coded in the microcontroller firmware (the inverse procedure is



UNIONE EUROPEA
Fondo Sociale Europeo
Fondo Europeo di Sviluppo Regionale

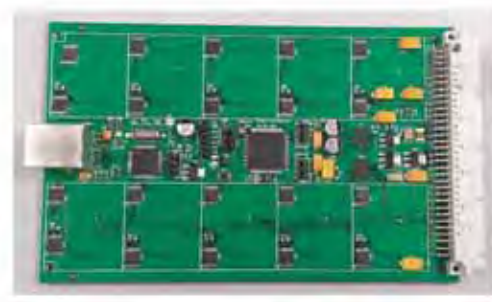


Fig. 43. INAF LNA monitoring&control bias board: 3D drawing (left) and photo of real board (right).

Item	Values
N. of amplification stages	10 (5 per polarization channel)
Drain voltage range	$0 \text{ V} \leq V_d \leq 5 \text{ V}$
Gate voltage range	$-6.5 \text{ V} \leq V_g \leq 5 \text{ V}$
Maximum drain current	$I_{dmax} \leq 50 \text{ mA}$ (per channel)
Max total power consumption	$\approx 5 \text{ W}$
ADC characteristics	16 bit with $\approx 15 \text{ Hz}$ sampling rate
Voltage resolution setting	$\approx 5 \text{ mV}$
Communication port	Auto-negotiated 100 Mb LAN with RJ45 connector
Board size (without front panel)	$h=100 \text{ mm}$, $\text{depth}=160 \text{ mm}$

Table 4. Main specification on the new INAF digital LNA board (GAIA).

applied when switching off). The same board includes Analogue to Digital Converters (ADCs) for remotely monitoring V_d , V_g , I_d for each of the 10 channels. Table 4 shows a list of the main specification of GAIA. The rack-mountable board is electrically and mechanically compatible with the ALISRT analogue board version. The digital board was designed to provide high bias voltage stability and to generate low RFI emission. Preliminary tests confirm the electromagnetic compatibility of the board, which is suitable for use at SRT.

Fig. 44 illustrates a 3D sketch of a standard 3U×19-inch rack mounting seven new digital LNA bias boards. The rack includes seven DC connectors (for example 27-pole from Fisher) and a power supply. For example, one single rack of this type could bias the LNAs of a W-band multibeam in 4×4 configuration requiring biasing of $4 \times 4 \times 2 \times 2 = 64$ amplification stages (16 feeds, dual polarization, two cryogenic LNA modules per polarization channel) where we suppose that one LNA module requires only one V_d and only one V_g .

The number of wires required to bias the LNAs (or “active OMT”) will be optimized by the supplier by minimizing their number when accounting for the specification on receiver noise, power consumption and electrical/mechanical consideration.

The optimization of LNA bias wires can be achieved, for example, by grouping the voltages of multiple stages inside the same LNA module and/or of different LNA modules.

The number of wires/voltages will determine the number of required LNA bias board.

A chord with multiple DC wires will connect the multipole connectors of the LNAs rack to the vacuum feedthrough DC connectors (for example 27 poles from Fisher) to be placed on the cryostat backplate.



UNIONE EUROPEA
Fondo Sociale Europeo
Fondo Europeo di Sviluppo Regionale

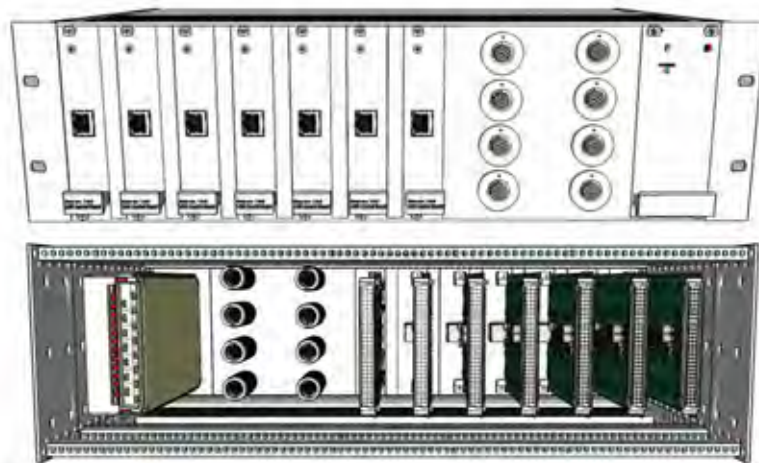


Fig. 44. Sketch of a standard 3Ux19-inch rack with seven new digital LNA bias boards, DC connectors and power supply.

7.4 DOWN-CONVERTER MODULE(S)

The frequency down-converter could consist of one or more modules and should be designed to be compatible with the electrical and mechanical interfaces that will be available at the cryostat backplate, where cryocooler, vacuum pump, vacuum gauge, DC bias connectors and other electrical/mechanical parts will be located. If waveguide band pass filters (BPFs) are employed at the cryostat backplate (see receiver architectures illustrated in Fig. 5 and Fig. 28) the down-converter will interface at its input with such waveguide filters.

A 3D sketch of four possible down-converter modules placed on the cryostat backplate of a 4x4 SSB receiver is shown in Fig. 45.

Each module has eight waveguide inputs, one 11.33-16.33 GHz LO input signal and delivers eight 2-18 GHz 1IF output. The module architecture, based on Schottky semiconductor mixers, refers to Fig. 28. The local oscillator is distributed internally to each module by an eight-way LO splitter. The DC connector, the chord for biasing the down-converter internal components (sextupler, power amplifiers, mixers, LNAs, etc.) and the four-way LO power splitter that feeds the four different modules are not shown in the sketch of Fig. 45.

The 11.33-16.33 GHz LO input signal will be provided by a master synthesizer available on the SRT antenna. The synthesizer is phase-locked to the antenna maser. The synthesizer is not part of the supply, but it is required for testing the W-band receiver.

Alternative down-converter designs are possible. For example, the down-converter might use a single module with: *a)* 32 waveguide inputs (18 for the 3x3 array); *b)* one LO input; *c)* 32x1IF coaxial cable outputs (36 for the 2SB 3x3 array); *d)* a single DC bias connector with bias chord. The down-converter waveguide inputs would interface to the waveguide feedthroughs mechanical vacuum flange on the cryostat backplate illustrated in Figs. 38 and 39.

The downconverter active parts (mixers, frequency multipliers, LNAs, power amplifiers, etc.) will be biased using power supplies located in a rack of the electronics cabinet. The bias wires chords will connect the downconverter to the power supply. Remote

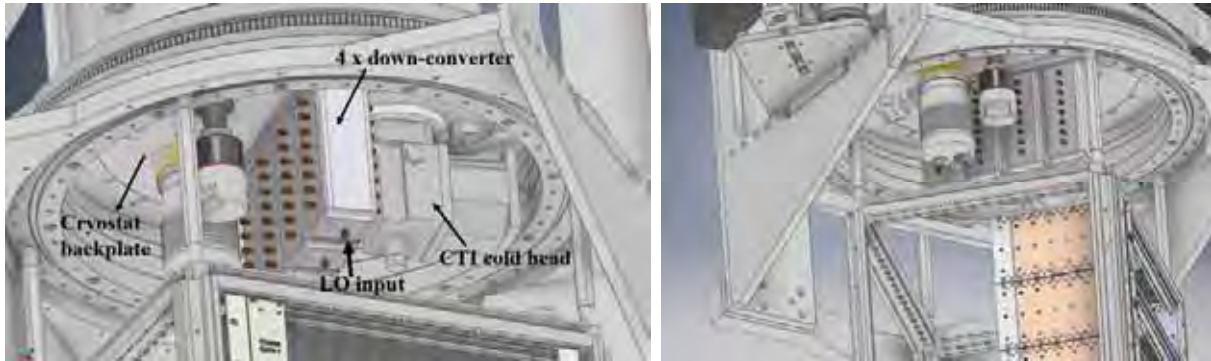


Fig. 45. 3D sketch showing the four independent downconverter modules attached to the cryostat backplate, which must also host the vacuum valve (not shown), the turbomolecular vacuum pump, the vacuum gauge, the CTI cryogenerator and the vacuum feedthrough DC connectors (not shown) for biasing the internal components of the cryostat.

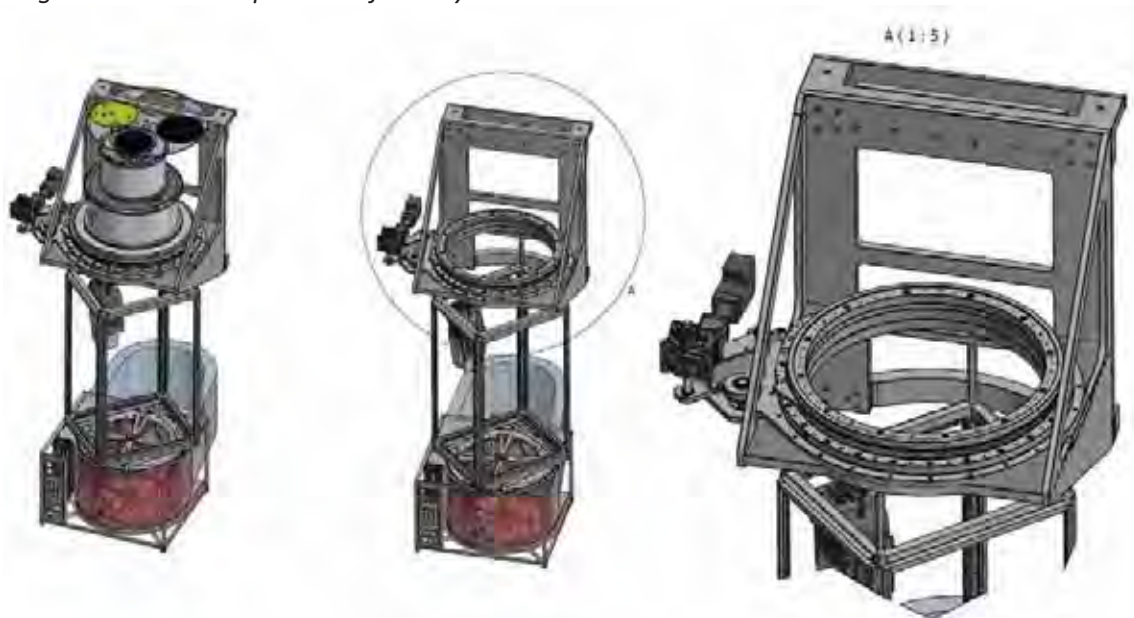


Fig. 46. 3D sketch of the derotator with mechanical support structure and (empty) electronics cabinet.

monitoring and control of the bias values of the active parts of the down-converter is not a requirement. The supplier can decide whether or not to implement it. The LNA bias board developed by INAF could in principle be used also for biasing the downconverter module.

7.5 MECHANICAL DEROTATOR AND DEWAR INTERFACE

The receiver shall include a mechanical derotator to maintain the parallactic angle during source tracking, as described in Sec. 4.1. The 1IF cable wrap with ≈ 4 m long 1IF coaxial cables and helium lines for the cryogenerator are considered part of the derotator mechanism. The derotator will be attached to the external part of the cryostat. Drawings of the derotator mechanism are illustrated in Fig. 46. INAF will provide the drawings of the derotator and its remote monitoring and control system, which must be supplied with the receiver.



7.6 SOLAR FILTERS/CALIBRATION SELECTOR

The solar filter and calibration wheel must be remotely controlled by a motor. The wheel can be fixed either on the cryostat or on the external mechanical support. In the latter case, the filters and calibrator would rotate with respect to the feed-horn array during source tracking (while the receiver is rotated by the derotator). The wheel mechanism has four positions: 1) blank through pass; 2) solar filter centred at 78 GHz; 3) solar filter centred at 110 GHz; 4) 293 K calibrator. Magnetic Reed sensors or encoders interlock can be used to read the wheel position.

7.7 NETWORK AND REMOTE COMMUNICATION

The multibeam receiver shall be monitored and controlled through the SRT software (see <http://discos.readthedocs.io/en/latest/> and <http://discos.readthedocs.io/en/latest/>). Most of the receiver sub-systems require a network connection for communication, monitoring and control. These are summarized in Table 5.

Item	Number of RJ45 ports
Mechanical derotator	1 port
Cryogenic LNA bias boards	TBD (two for ALISRT, seven for GAIA)
Cryogenic and vacuum control	1
Down-converter	TBD
Local Oscillator	1
Solar filter/calibration switching wheel	1
Maintenance empty ports	2

Table 5. W-band multibeam receiver parts that must be monitored and controlled through the SRT software.

An Ethernet switch with a sufficient number of RJ45 ports and at least two SFP ports with optical transceivers (multi-mode) need to be connected for communication, monitoring and control. The Ethernet switch must be RFI-compatible (to be tested) and provided along with the receiver. INAF can suggest Ethernet switches that has already tested.

7.8 RECEIVER SUB-SYSTEM DESIGNS PROVIDED BY INAF

The following drawings/designs will be provided (upon request) to the companies/consortia (economic operators) that will qualify to the final award phase of the tendering under a Non-Disclosure Agreement (NDA):

- mechanical derotator;
- receiver monitoring and control electronics;
- feed-horns and of OMTs;
- preliminary drawings of the cryostat.



UNIONE EUROPEA
Fondo Sociale Europeo
Fondo Europeo di Sviluppo Regionale



8 Summary of receiver minimum requirements

Table 6 summarizes the minimum top-level requirements for the W-band multibeam receiver. The detailed specifications will be determined during the competitive dialogue. The table provides a list of all hardware and software components to be delivered. The receiver shall be monitored and controlled using the SRT control software.

Array receiver specification	Value
Baseline RF band (GHz)	75-116
Goal RF band (GHz)	70-116
Polarization properties	Two orthogonal linear polarizations, named H & V, shall be available Circular polarization is an option but not a requirement.
Number of beams and array configuration	Minimum 9 beams in square 3 x 3 configuration. Goal 16 beams in square 4 x 4 configuration. Intermediate configurations (i.e. 3 x 4 or others) are possible (TBD).
Angular spacing in the sky between contiguous beams	23" to 62" (HPBW≈12" at 100 GHz)
Ratio beam-spacing/HPBW	2 to 5.5 at all frequencies
Mechanical derotator	Required to maintain the parallactic angle during source tracking. Shall include the servo-system and encoder controllable by the SRT "Nuraghe" control software. Angular rotation +/- 120 deg. Rotation speed shall allow derotation while tracking sources up to an antenna elevation of 85 degrees. Drawings by INAF.
Mechanical frame	Yes, to mount the receiver on the Gregorian focus rotating platform. Drawings by INAF.
Illumination Taper for each of the feeds (dB)	≈-12 @ 12° sub-reflector edge half-angle at 93 GHz (central frequency). INAF feed drawings available upon request under NDA.
Maximum gain loss for off-axis feeds compared to central feed at all frequencies (dB)	-1
Return loss (dB)	>15 (at input of all feed-horns and OMTs)
Crosspol (dB)	< -25 (at any frequency within the receiver tuning range, the cross-polarized component for each of the two polarization channels shall be at least 25 dB below the desired co-polar signal component)
Receiver calibration	Yes, for all receiver chains. One single room temperature (296 K) calibration load. More complex alternatives are possible, including two-load calibration, external injection by noise diode from sub-reflector Alternative and injection through waveguide coupler before the cryogenic LNAs.
Sun observation	Yes, at 78 GHz and 110 GHz (non-simultaneous). Band pass filters could be adopted in front of the receiver vacuum window. Alternative receiver chain designs include use of high P1dB compression point components.
LO1 frequency	Tunable at fundamental or sub-harmonic frequency across ≈10-20 GHz, via high phase stability synthesizers locked to the maser station. Provided by INAF.
Phase and amplitude stability	Determined by the synthesizers and multiplication chain
First down-converter	Based on Sideband Separating Mixer (2SB) scheme or on Single Side Band Mixer scheme
IF1 frequency band and range (GHz)	Baseline: 12 GHz per pixel per polarization. Two 6 GHz-wide bands across 4-12 GHz for 2SB or one 12 GHz-wide band across 2-18 GHz. Goal: 16 GHz per pixel per polarization. Two 8 GHz-wide bands across 4-12 GHz for 2SB or one 16 GHz-wide band across 2-18 GHz.
Number of IF1 outputs from first down-converter modules	Minimum 18 (9 pixels × 2 polarizations × one 1IF band if 2-18 GHz SSB config.); Other options include: 36 (9 pixels × 2 polarizations × two 1IF sidebands if 4-12 GHz 2SB config); 32 (16 pixels × 2 polarizations × one 1IF band if 2-18 GHz 2SB config); Maximum number of 1IFs: 38 (set by the RFoF optical links and FBCB)
1IF output power and flatness	TBD (≈-30 dBm if the receiver looks at a 296 K cal load).



UNIONE EUROPEA
Fondo Sociale Europeo
Fondo Europeo di Sviluppo Regionale



	TBD (<8 dB full band if 1IF 4-12 GHz). TBD (<13 dB full band if 1IF 2-18 GHz).
Image sideband rejection for first down-converter (dB)	TBD (R> 10)
Intermodulation products and level of unwanted LO harmonics	TBD (as low as possible, best effort); unwanted harmonics TBD (<-30 dBc)
Cryogenic LNAs or active "OMT"	From commercial companies or research institutions
Cryogenic LNA gain (dB)	TBD (expected ≈45 dB in the cryostat)
Cryogenic LNA gain flatness	TBD (as flat as possible, best effort). It affects the receiver sideband rejection.
RX noise temperature (K)	< 70 K (measured in front of vacuum window for all sub-bands)
Gain of the first down-converter (dB)	TBD
Gain saturation	The large signal gain compression shall be less than 5% between the situation that a 77 K load is placed at the RF input port and the situation that a 300 K load is placed at the same RF input port.
Waveguides, connectors and interfaces	TBD
Electromagnetic compatibility	The receiver and its sub-system shall not generate Radio Frequency Interference
VACUUM and CRYOGENICS	
Vacuum level (mbar)	10^{-6} - 10^{-7}
Cold head	One CTI Cryogenics, either model 350 or 1020 (compatible with available compressors)
Compressor	CTI 9600 (not to be supplied)
Temperature at stages	1 st stage : < 80 K typical, 2 nd stage : < 20 K typical
Temperature Monitor	Yes, on both cryogenic stages (four in total). Model by INAF.
Vacuum Sensor and Monitor	Yes, and remote control of vacuum valve. Model by INAF.
PHYSICAL	
Dewar diameter (mm)	≤ 590
Overall diameter (mm)	< 800 (a bigger diameter is allowed below the Gregorian focus)
Height (mm)	≤ 2465
Weight (kg)	< 250
ENVIRONMENTAL	
Ambient Temp. and RH	RXs are located in air-conditioned room
ORIENTATION	
	The receiver shall meet all performance requirements over a range of gravity vectors from 0 to 90 degrees (antenna elevation angles)
PRIMARY POWER	
1. Voltage (V)	230
2. Frequency (Hz)	50
Consumption (W)	TBD
MONITOR and CONTROL	
	To switch on/off cryocooler, vacuum, LNAs bias, mechanical derotator, compatible with the SRT control software.
MTBF and LIFETIME	
MTBF	The Mean Time Between Failure of the receiver shall exceed 20 years
Lifetime	The receiver minimum lifetime shall be 15 years from date of delivery
Delivery time, installation and pre-commissioning validation	
Delivery period	Expected: On-site acceptance test at the supplier facility 21 months after contract signature;
Installation on SRT telescope and instrument pre-commissioning validation	Delivery to SRT and installation 22 months after contract signature. Installation with support from local INAF SRT team.
Spare parts	Yes, to guarantee full operation of the instrument for at least 10 years after installation



UNIONE EUROPEA
Fondo Sociale Europeo
Fondo Europeo di Sviluppo Regionale



Spare of active components	Yes. Parts and quantities TBD (LNAs, first down-converter sub-parts, etc.)
Spare of passive components	Yes, Parts and quantities TBD (one additional feed, OMT and waveguide filter)

Tab. 6. Top-level preliminary specification of 3 mm band multibeam receiver

9 Conclusions

We presented the baseline specification of the W-band multibeam heterodyne receiver for the SRT Gregorian focus, provided an advanced design study carried out at INAF of the instrument which can be used in support of the work to be carried out by the interested economic operators. Furthermore, we provided the details of the hardware and of the monitor&control software that must be adopted for the receiver to comply with the existing SRT telescope interfaces.



UNIONE EUROPEA
Fondo Sociale Europeo
Fondo Europeo di Sviluppo Regionale



APPENDIX A: SRT science with the W-band multibeam receiver

A 3 mm band heterodyne multibeam receiver operating on the SRT will constitute a valuable resource for the entire international scientific community. The collecting area of the SRT combined with the array will allow fast mapping of extended, low-brightness sources with an angular resolution $\sim 12''$. It will be possible to carry out simultaneous observation of continuum emissions and spectral lines, using both a total power backend and high-spectral resolution digital backends (provided by INAF).

A list of the main instrument science driver is provided below:

- a) Multi-spectral line observations of both compact and diffuse low-temperature molecular gas typical of the interstellar medium and of star-forming regions. The mapping of molecular species such as $\text{HCO}^+/\text{HCN}/\text{HNC}$, SiO , CH_3OH , CS and their isotopologues, will allow studying the kinematics and the chemistry of these regions. In particular, in the last years star-formation studies have concentrated on the modeling and observations of the molecular “filaments”, which SRT will be able to map with a linear resolution similar to their typical width, i.e., ~ 0.1 pc. We will also be able to study the so-called interstellar “bubbles” detected at infrared wavelengths, in order to better understand the physical processes that generate them;
- b) The ability to observe various molecular gas tracers simultaneously will significantly advance the study of star formation in nearby galaxies, by analyzing for example the relationship of the most abundant gas tracer (e.g., CO , HCO^+ , HCN , HNC) to other signposts of star formation. W-band observations will also allow correlating star formation rates in different types of galaxy with the abundance of CO , HCN and other molecular tracers. The wide instantaneous receiver frequency range and the new digital spectrometer will also allow to detect $^{12}\text{CO}(1-0)$ and $^{13}\text{CO}(1-0)$ in high-redshift galaxies;
- c) Mapping of the radio emission from the Sun and use of these observations for space weather applications.

The atmospheric monitoring at the SRT site and the models employed to estimate the attenuation and variability of the signal due to the atmosphere have shown that it will be possible to carry out observations in the 3 mm band for a significant fraction of the operating time, mainly during the winter season. The possibility of observing with a large bandwidth is fundamental to reduce the mapping time during spectro-polarimetric imaging of extended sources and during spectral surveys. The atmospheric opacity fluctuations in W-band require relatively short observing time to optimize the calibration process and the scientific results in terms of observing parameters (sensitivity and reduction of systematic effects due to atmospheric variability during the observation). A receiver with at least nine feeds will allow high- spatial resolution surveys in regions of the sky with angular size of a few arcminutes in



UNIONE EUROPEA
Fondo Sociale Europeo
Fondo Europeo di Sviluppo Regionale



relatively short observing time. The operational parameters of the receiver will be determined during its scientific validation phase through specific observing campaigns aiming at establishing the observational performance of the instrument.

Depending on the chosen down-conversion scheme, the receiver will be capable of observing across the entire 70-116 GHz frequency band with only three or four frequency tunings.

Thanks to the installation of the heterodyne multibeam receiver, SRT will be one of the few single-dish radio telescopes in the world capable of carrying out high-sensitivity spectro-polarimetric astronomical observations across the 3 mm band, making of it an almost unique facility in the international context.

APPENDIX B: SRT optics

Fig. B1 shows the detailed optical parameters of the SRT.

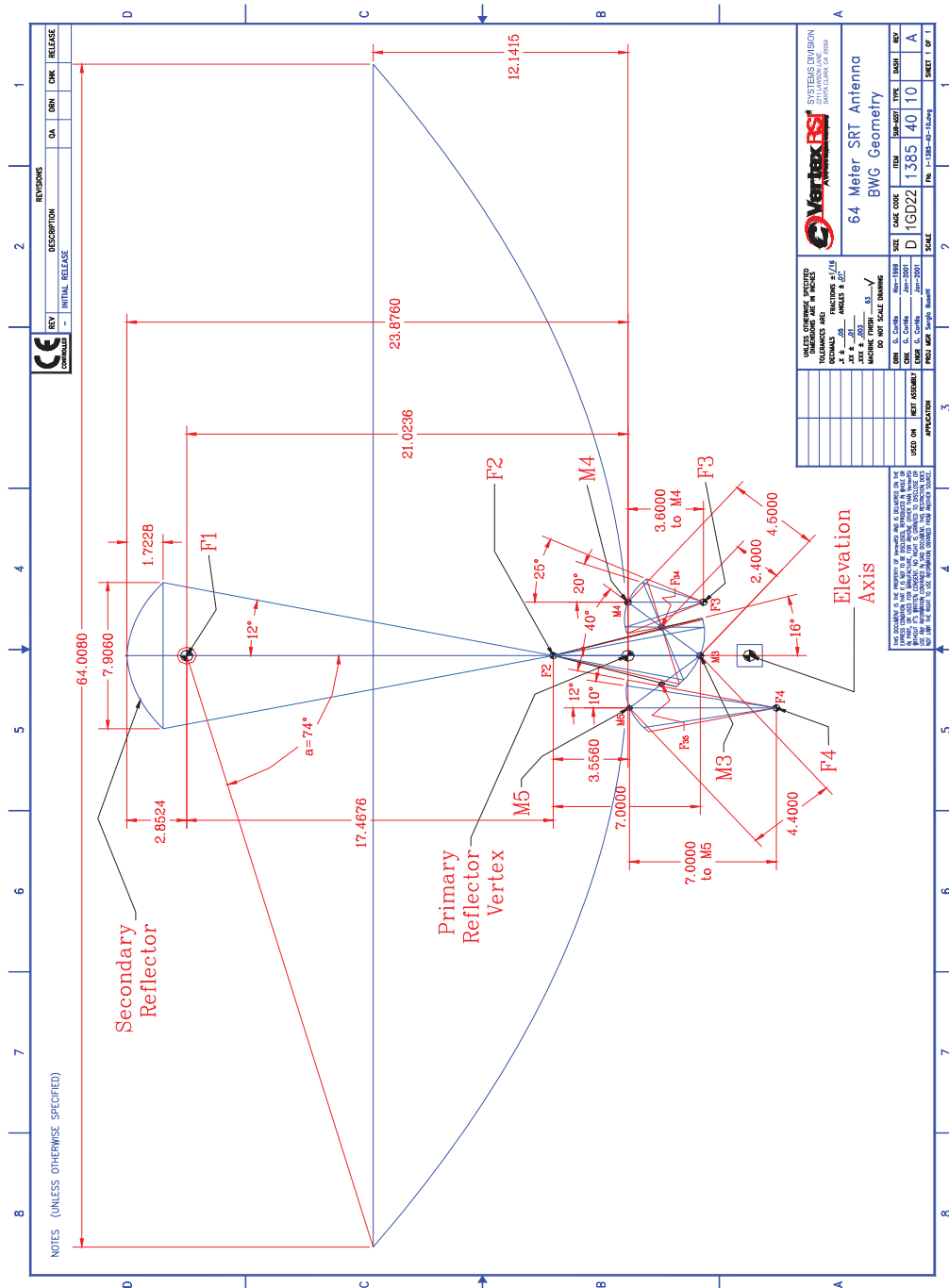


Fig. B1. Optical parameters of the SRT antenna.



UNIONE EUROPEA
Fondo Sociale Europeo
Fondo Europeo di Sviluppo Regionale



Electromagnetic simulation of 3×3 array optics across 70-116 GHz

We used the Grasp software to perform electromagnetic simulations of the array receiver coupled with the SRT optics. These simulations assumed the SRT shaped surfaces and the array placed at the Gregorian focus. We used the GTD (Geometrical Theory of Diffraction) method to model the secondary mirror and the PO (Physical Optics) method to model the primary reflector. The modeling accounts for the radiation patterns of an illuminating diffraction-limited feed-horn optimized for operation across the full 70-116 GHz bandwidth. The illuminating feed horn has an internal aperture diameter of ≈ 21 mm and an external diameter of ≈ 31 mm. The feed spacing is assumed to be 45 mm.

Figure B1 (see also Fig. 14) shows the array geometry where the feeds are color-coded based on their distance from the optical axis. Table B1 provides the results of the electromagnetic simulation for the on-axis feed and for the off-axis feeds n. 2, 3. At 93 GHz, the central frequency of the 70-116 GHz band, the drop of the antenna gain for feed n. 3, which is located at one of the vertices of the square, is approximately 10% of the on-axis value. This loss is 18 % at 116 GHz (lower than the maximum acceptable level of 20%) and 4.7% at 70 GHz.

Fig. B2, left panel, shows a possible scanning geometry of the array used for mapping large angular areas in the sky. A nearly Nyquist-sampling (0.59 HPBW offset) is achieved at 116 GHz with three sub-scans (right panel). The profiles shown on the left of each panel represent the overlapping level of all the combined beams. Fig. B2, right panel, shows that a uniform sampling can be achieved with three sub-scans. At the lowest frequency of the band, 70 GHz, the HPBW is ≈ 15 arcsec, and a Nyquist oversampling (0.45 HPBW) would be achieved if using the same scanning configuration.

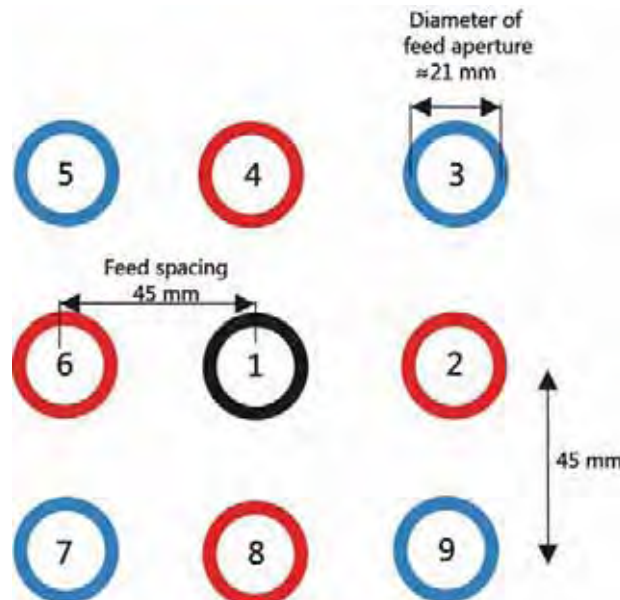


Fig. B1. Configuration of the 3×3 array with 45 mm spacing between contiguous feeds. The diameter of the feed aperture is about 21 mm.



Optical parameters of 3x3 multifeed with 45 mm feed spacing illuminating the SRT from the Gregorian focus (simulated with Grasp software)				
Frequency [GHz]	70	93	100	116
Gain CoPolar [dBi]	91.50	94.68	95.02	95.14
	91.38	94.42	94.71	94.62
	91.27	94.19	94.44	94.20
3dB BeamWidth [arcsec]	15.23	12.38	11.95	11.59
	15.19	12.35	11.88	11.30
	15.08	12.20	11.74	11.27
Angular offset from optical axis θ [arcsec]	0.00	0.00	0.00	0.00
	62.24	62.07	61.98	61.65
	87.96	87.80	87.72	87.42
Pointing direction ϕ [deg]	0.00	0.00	0.00	0.00
	0.00	0.00	0.00	0.00
	45.07	44.98	44.93	44.71
Antenna efficiency ⁶ [%]	64	76	71	54
	62	71	66	48
	61	68	62	44
Gain loss with respect to illumination with central feed [%]	0.0	0.0	0.0	0.0
	3.1	6.6	7.0	11.1
	4.7	10.5	12.7	18.5
Cross-polarization level [dB]	-48.82	-39.22	-38.33	-35.73
	-43.67	-38.67	-37.91	-34.84
	-47.85	-38.43	-37.55	-34.16

Table B1. Grasp simulation of the SRT Gregorian optics illuminated by the array of feeds shown in Fig. B1. Black refers to the on-axis feed, red to feed 2 and blue to feed 3.

⁶ The values of the antenna efficiency in Table B1 assume no deviations from the ideal optical surfaces. When accounting for a Ruze error distribution due to a surface rms of order 180 μm (goal to be achieved with an active primary surface and a metrology system) the antenna efficiency is reduced by a factor of ≈ 2 .



UNIONE EUROPEA
Fondo Sociale Europeo
Fondo Europeo di Sviluppo Regionale

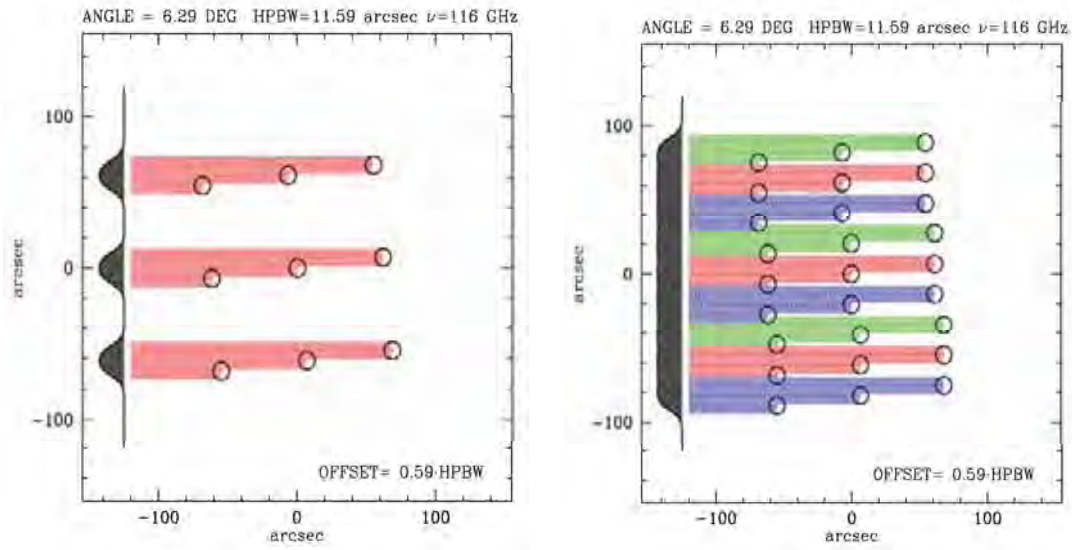


Fig. B2. Scanning geometry with the 3x3 array for mapping at 116 GHz. The array is oriented at an angle of ≈ 6 deg with respect to the scanning direction. Three sub-scans with 0.59 HPBW offset allow achieving near-Nyquist sampling of the source. The overlapping of the beams is shown on the left of each panel (courtesy of M. Murgia).



UNIONE EUROPEA
Fondo Sociale Europeo
Fondo Europeo di Sviluppo Regionale



APPENDIX C: SRT atmospheric site characterization and monitoring

The quality of radio telescope observations depends on the atmospheric conditions. Millimeter wavelengths are affected by the extremely variable atmospheric water vapor content and by the weather conditions in general. INAF utilizes various tools and sensors to: characterize the SRT site (statistical analysis); support the observations (nowcasting of atmosphere parameters); plan and schedule the observation (forecasting of the parameters of interest).

The adopted tools and sensors are:

- a) A statistical analysis of over 50-year long radiosondes data (launching site is the airport of Cagliari, 35 km away from the SRT) provides vertical profiles of temperature relative humidity, pressure, and water concentration up to the troposphere upper limit. A radiative transfer model is used to evaluate the Integrated Water Vapour (IWV), sky opacity and system noise temperature.
- b) ground-level meteorological sensors;
- c) a microwave radiometer (Radiometrics MP3000A) with 35 selectable channels, in 22-30 and 51-59 GHz bands provides in real-time IWV, opacity and vertical profiles of temperature, humidity, vapor and liquid content up to 10 km of height.
- d) geodetic GPS as a non-conventional atmospheric probe. The GPS signal is delayed (path delay) by the atmosphere components. This path excess may be accurately measured by the GPS. The IWV is obtained from the path delay in real-time. INAF operates a regional network of GPS permanent stations. The network estimates in real-time the IWV and delivers 2D maps of such parameter.
- e) Local area models (LAM): Accurate weather predictions may increase the antenna performances at high frequencies. The forecasts are mandatory for the implementation of a dynamic scheduling system through which the observations are scheduled accordingly to the oncoming weather scenario. INAF adopts a high spatial resolution LAM to predict, 48 hours in advance, the integrated water vapor (accuracy < 3 mm), the atmospheric opacity, rain and surface winds.

The analysis results are illustrated in Figs. C1-C3 (courtesy of F. Buffa).

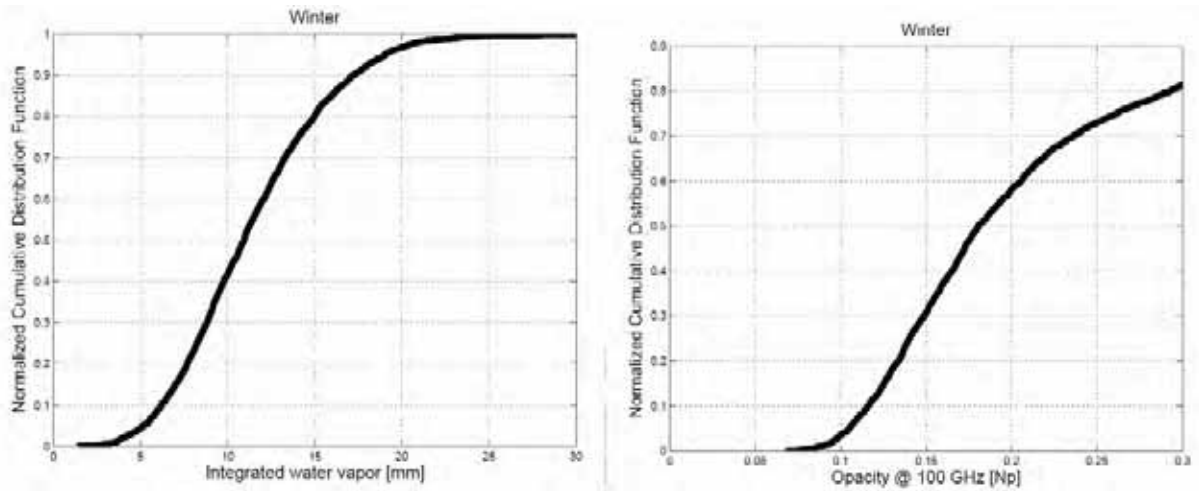


Fig. C1. Integrated water vapour distribution function (left panel) and 100 GHz opacity (right panel) at the SRT site during Winter season.

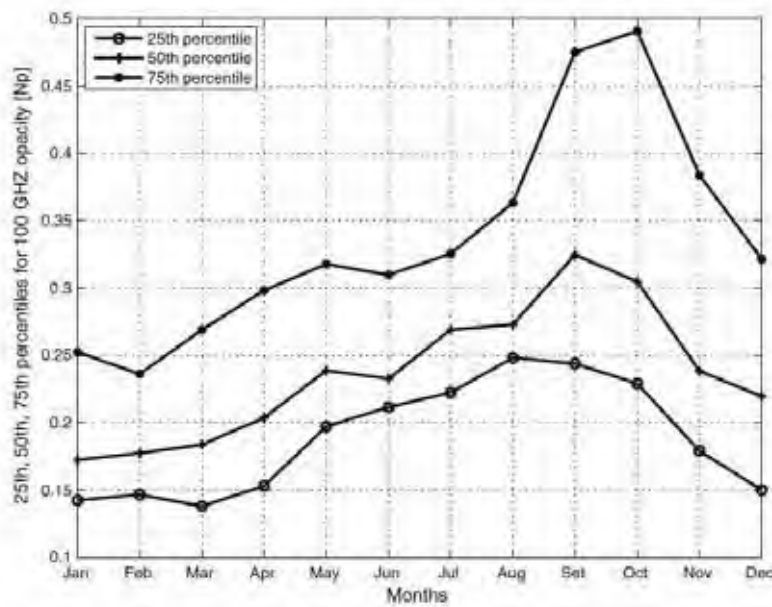


Fig. C2. Percentile 100 GHz opacities at the SRT over 12-month timescale.



UNIONE EUROPEA
Fondo Sociale Europeo
Fondo Europeo di Sviluppo Regionale

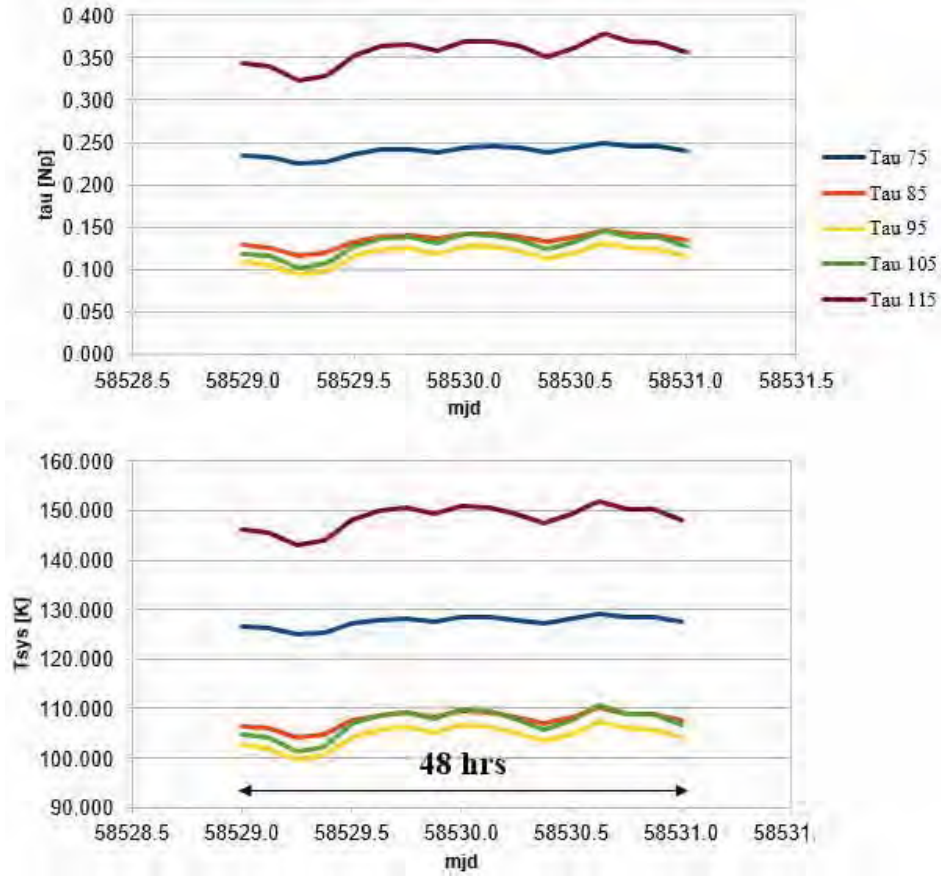


Fig. C3. Predicted zenith absorption (top panel) and system noise temperature (bottom panel) at the SRT site over 48-hour period (in modified Julian day - mjd) based on Local Area Model for the days of Feb 16-17, 2019. The T_{sys} prediction is based on the assumption that $T_{rec}=50$ K and refers to the Zenith.



UNIONE EUROPEA
Fondo Sociale Europeo
Fondo Europeo di Sviluppo Regionale



APPENDIX D: W-band receiver array architectures

The main technical selection criteria will be based on the proposed number of pixels, RF and IF bandwidths, receiver noise temperature and sideband rejection ratio. The following list provides a sample of possible array architectures in increasing order of scientific relevance.

- 1) 3x3 pixel, 2SB, 2×4 -12 GHz 1IF bands per polarization channel (36×1 IF outputs);
- 2) 3x3 pixel, SSB, 1×2 -18 GHz 1IF band per polarization channel (18×1 IF outputs);
- 3) 3x4 pixel, SSB, 1×2 -18 GHz 1IF band per polarization channel (24×1 IF outputs);
- 4) 4x4 pixel, SSB, 1×2 -18 GHz 1IF band per polarization channel (32×1 IF outputs);

The sideband separating scheme (2SB), similar to the one adopted for the AETHRA WP1 receiver, is the baseline specification for the SRT. However, we would prefer to adopt the single sideband (SSB) scheme delivering 2-18 GHz IF band per each of the polarization channels (i.e. one single 2-18 GHz IF band instead of 2×4 -12 GHz bands). There would be two advantages in the SSB down-conversion scheme:

- a) the number of IF outputs to transport for the 4x4 SSB receiver (32×2 -18 GHz IF outputs) would be compatible with the number of analogue fiber-optic links that will be available from the SRT Gregorian room to the backend room (a maximum of 38 optical links will be available). Instead, for a sideband separating scheme an additional IF selector would be required to reduce the number of 1IFs from 64 to 32.
- b) the 2-18 GHz IF band could be fully processed by the analogue backend that INAF will develop and install in the backend room and that will be common to all the Gregorian focus receivers (including the W-band). The analogue backend will divide the 2-18 GHz 1IF band into eight sub-bands (named B1-B8, see Fig. 26) and will not be part of the W-band receiver contract. Its development will be in charge to INAF.



UNIONE EUROPEA
Fondo Sociale Europeo
Fondo Europeo di Sviluppo Regionale



APPENDIX E: Second down-converter (FBCB) and W-band receiver observing modes

We describe the FBCB and the possible observing modes with the W-band multibeam receiver. This section is extracted from the INAF internal report [8]. A schematic of the second down-converter stage for one of the two polarization channels, to be developed by INAF, is shown in Fig. E3. The second down-converter is part of the FBCB (Full Band Conversion/Continuum Board/Back-end) to be developed by INAF and must not be provided by the supplier of the W-band receiver. The FBCB will be based on various FBCB microwave boards and will be shared with other Gregorian focus receivers, as shown in Fig. 30.

One FBCB board has two 2-18 GHz 1IF inputs (two polarization channels, Pol H and Pol V for one feed) each of which is separated into eight 2 GHz sub-bands named B1, B2 ... B8, where the covered sub-bands refer to B1=2-4 GHz, B2=4-6 GHz ... B8=16-18 GHz (see also Fig. 29). In total, one FBCB board delivers 8 sub-bands for Pol H and 8 sub-bands for Pol V.

The FBCB will manage up to 38×2 -18 GHz (1IF) inputs and divide each of them in 8×2 GHz sub-bandwidths (Band 1 to Band 8). The number 38 is set by the Q-band 19-element dual polarization receiver under development by INAF.

A W-band receiver in 3×3 4-12 GHz 1IF sideband separating configuration (option n. 1 of Appendix D, corresponding to Fig. 5 receiver architecture) delivers 36×1 IF signals to the FBCB. The FBCB will deliver 144×2 GHz-wide sub-bands at its output.

A 4×4 SSB W-band receiver with 2-18 GHz 1IFs (option n. 4 of Appendix D, corresponding to Fig. 28 receiver architecture) delivers 32×1 IFs signals to the FBCB. The FBCB will deliver 256×2 GHz-wide sub-bands to its output.

Only a sub-set of the outputs of the FBCB is delivered to the backends. The possible observing modes that will be available with two W-band receiver configuration are presented.

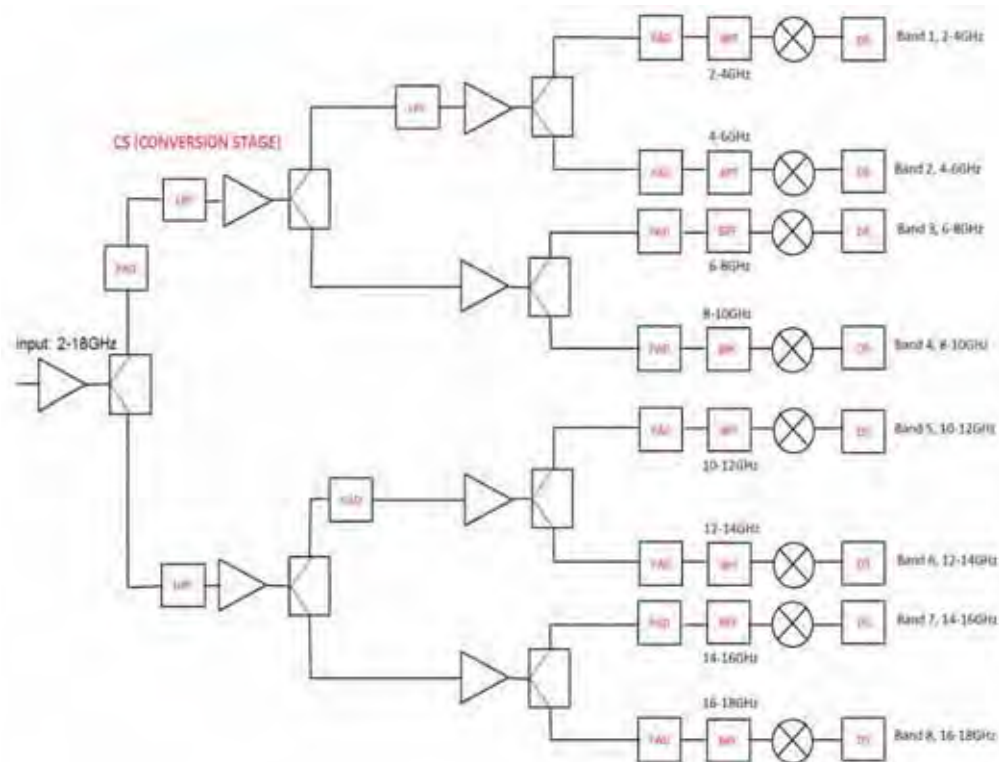


Fig. E1. Schematic of the conversion stage of the FBCB board under development at INAF. Only one of the 1IF inputs is shown.

E1. OBSERVING MODES FOR 3×3 2SB RECEIVER ARCHITECTURE

The total 1IF band for each polarization is 16 GHz, 8 GHz per sideband across 4-12 GHz (the USB and the LSB). Thus, only the sub-bands B2, B3, B4, B5 are delivered at the output of the FBCB, the others B1, B6, B7 and B8 are unused. Five different observing modes would be available:

Mode A: 9 feeds, 2 polarizations, 2 sub-bands per polarization

H-pol: choice of one among B2, B3, B4, B5 of the USB and one among B2, B3, B4, B5 of the LSB; the chosen pair would be the same for the 9 feeds;

V-pol: choice of one among B2, B3, B4, B5 of the USB and one among B2, B3, B4, B5 of the LSB; the chosen pair would be the same for the 9 feeds;

Mode B: 9 feeds, 4 sub-bands

This is mode A, where of the 4 sub-bands, two are on one polarization channel and two on the other polarization channel. For example, B2_H_LSB and B3_V_LSB and B4_H_USB B5_V_USB. It is possible to choose 4 contiguous sub-bands. This mode is used when the observation does not require to discriminate the polarizations.

Mode C: 1 feed, 2 polarizations, 8 sub-bands per polarization

One of the feeds must be chosen (for example the central feed, feed 1).

H-pol: the following sub-bands are available B2 AND B3 AND B4 AND B5 USB AND B2 AND B3 AND B4 AND B5 LSB

V-pol: the following sub-bands are available B2 AND B3 AND B4 AND B5 USB AND B2 AND B3 AND B4 AND B5 LSB

Mode D: 5 feeds, 2 polarizations, 4 sub-bands per polarization

Choose one sub-band among B2 and B4 along with one among B3 and B5 for both USB and LSB, for both polarizations (see Fig. E2).

H-pol: chose one among B2, B4 USB AND one among B3, B5 USB AND one among B2, B4 LSB AND one among B3, B5 LSB. The two couples will be the same for all feeds.

V-pol: chose one among B2, B4 USB AND one among B3, B5 USB AND one among B2, B4 LSB AND one among B3, B5 LSB. The two couples will be the same for all feeds; the couple chosen for Pol-V could be different from Pol-H.

If the polarization is not of interest it is possible to observe all of the 8 sub-bands.

Mode E: 3 feeds, 2 polarizations, 4 sub-bands per polarization

Another option, identical to Mode D, can be obtained with three aligned feeds 1, 2, 6 to track the same elevation and use a dual-feed or a tri-feed configuration for the atmospheric calibration. See Fig. E2.



Fig. E2. Subset of W-band feeds used for observing modes D and E.



UNIONE EUROPEA
Fondo Sociale Europeo
Fondo Europeo di Sviluppo Regionale



E2. OBSERVING MODES FOR 4×4 SSB RECEIVER ARCHITECTURE

The 16 GHz 1IF band (across 2-18 GHz) for each polarization channel can be used in full. A total of 9 FBCB boards would be used. The four following observing modes would be available:

Mode A: 16 feeds, 2 polarizations, 1 sub-band per polarization

H-pol: chose one among sub-bands B1, B3, B5, B7 or one among sub-bands B2, B4, B6, B8. The sub-bands will be the same for all of the 16 feeds;

V-pol: chose one among sub-bands B1, B3, B5, B7 or one among sub-bands B2, B4, B6, B8. The sub-bands will be the same for all of the 16 feeds. The chosen V-pol sub-bands could be different from the one of H-pol.

Mode B: 7 feeds, 2 polarizations, 2 sub-band per polarization

7 feeds, among the 16, must be chosen.

Pol-H: choose one among B1, B3, B5, B7 and one among B2, B4, B6, B8. The chosen couple will be the same for all of the 7 feeds;

Pol-V: choose one among B1, B3, B5, B7 and one among B2, B4, B6, B8. The chosen sub-band couple for all of the 7 feeds; The couple of Pol-V sub-bands can be different from the one of Pol-H.

Mode C: 7 feeds, 4 sub-bands

7 feeds, among 16, must be chosen.

Four different sub-bands are available, but not on only one polarization channel. This mode is similar to Mode B, where two sub-bands are on Pol-H and two on Pol-V.

The 4 sub-bands could be contiguous, for example: B3 and B4 of Pol-H and B5 and B6 of Pol-V, or B1 and B2 of Pol-H and B3 and B4 of Pol-V, etc.

Mode D: 2 feeds, 2 polarizations, 8 sub-bands per polarization

Two among the 16 feeds must be chosen (for example feed 1 and feed 2).

Pol-H: the following sub-bands are available B1 and B2 and B3 and B4 and B5 and B6 and B7 and B8, i.e. all sub-bands.

Pol-V: the following sub-bands are available B1 and B2 and B3 and B4 and B5 and B6 and B7 and B8, i.e. all sub-bands.

REFERENCES

- [1] A. Navarrini, A. Orfei, A. Scalambra, R. Nesti, L. Olmi, S. Leurini, "Top-level technical requirements: 3 mm band multibeam heterodyne receiver for the Sardinia Radio Telescope," INAF Technical Note, 29 May 2018.
- [2] A. Navarrini et al., "PON Grant, W-band multibeam receiver for SRT Gregorian focus: technical requirement" Presentation at the W-band multibeam Information Day, held at INAF-OA Cagliari on Feb. 20, 2019.
- [3] A. Navarrini et al., "Preliminary design study of the W-band multibeam heterodyne receiver for the Sardinia Radio Telescope Gregorian focus," To be published as INAF Internal Report, 2019.
- [4] 7. A. Orfei et al, "A Multi-Feed Receiver in the 18 to 26.5 GHz Band for Radio Astronomy," IEEE Antennas Propag. Mag. 52(4), 62, 2010.
- [5] P. Bolli and L. Olmi, "Allineamento del sistema ottico di SRT in configurazione gregoriana e BWG," INAF Internal Report, Feb. 2009.
- [6] R. Nesti, INAF-Arcetri Astrophysical Observatory, internal communication.
- [7] A. Navarrini, G. Valente, P. Serres, F. Schaefer, F. Thome, O. Garnier "Compact dual-polarization cryogenic receiver module for the 75-116 GHz band," Proc. Int. Conf. on Electr. In Advanced Appl. (ICEAA), 10-14 Sep. 2018.
- [8] A. Orfei, A. Scalambra, P. Marongiu, M. Poloni, G. Comoretto, A. Navarrini, A. Orlati, E. Carretti "Nuovo sistema di ricevitori a SRT e loro integrazione ai back-end," INAF-Internal report, May 15th, 2019.